Paper Number 1.2   COMPARISON OF OBSERVED, MM5 AND WRF-NMM MODEL-SIMULATED, AND HPAC-ASSUMED BOUNDARY-LAYER METEOROLOGICAL VARIABLES FOR THREE DAYS DURING THE IHOP FIELD EXPERIMENT

Steven Hanna[1], Elizabeth Hendrick[2], Lynne Santos[3], Brian Reen[4], David Stauffer[4], A.J. Deng[4], Jeffrey McQueen[5], Marina Tsidulko[5], Zavisa Janjic[5] and R. Ian Sykes[6]

[1]Hanna Consultants, Kennebunkport, ME; [2]Epsilon Associates, Maynard, MA; [3]Air Quality Associates, North Billerica, MA; [4]Penn State University, University Park, PA: [5]NCEP, Camp Springs, MD; [6]L-3Com/Titan, Princeton, NJ

1. INTRODUCTION AND BACKGROUND

Many authors have recommended that improvements be made to methodologies where meteorological inputs are prescribed for air quality models (e.g., Pielke and Uliacz 1997, Pielke 1998, Seaman 2000). Most air quality model applications involve releases of hazardous chemicals near the ground, and the subsequent transport and dispersion take place in the boundary layer, which has a typical depth of 1 or 2 km. However, most three-dimensional, time-dependent meteorological (Met) forecast models are focused more on predicting "weather" variables such as rainfall and maximum temperature, rather than wind profiles, mixing depths, and turbulence profiles, which are of use to air quality models. Note that the terms air quality model and transport and dispersion model are synonymous in the current paper.

Some researchers have evaluated the Met model predictions of boundary layer variables with observations (e.g., Pielke 1998, Cox et al. 2000, Seaman 2000, Hanna and Yang 2001). Wind speed, u, and direction, WD, and mixing depth, z_i, are often compared. It is found that there is a "minimum" uncertainty that is due to stochastic variations that cannot be simulated by current models. The minimum wind speed root mean square error (RMSE) is about 1 m/s (Seaman 2000 and Hanna and Yang 2001). The minimum wind direction RMSE is largest at small wind speed and decreases approximately inversely proportional to wind speed (the approximate relation is RMSE (WD) = $60\%/u$). The mixing depth RMSE is considered differently for daytime and nighttime conditions. Generally the RMSE for z_i is about 100 or 200 m for summer days with clear skies, when z_i is about 1000 m. For clear nights with light winds, the RMSE for z_i is of the same order as z_i itself (10 or 20 m). For windy conditions, the BL is nearly neutral day or night, and the RMSE for z_i is about 10 % of z_i. However, a caveat is that, about half of the time, the observed mixing depth is ambiguous because of the presence of clouds, residual boundary layers, unsteady conditions, advection, and other reasons.

The objective of this study is to develop improved meteorological (Met) inputs for the SCIPUFF transport and dispersion model, which was developed by Sykes et al. (2003) and is described and distributed as part of the Hazard Prediction Assessment Capability (HPAC) comprehensive modeling system by the Defense Threat Reduction Agency (2004). The paper focuses on analysis of mesoscale Met model outputs and comparison of the outputs with field experiment observations in the boundary layer (BL) and with SCIPUFF parameterizations of these variables. SCIPUFF requires inputs of Met variables such as wind speed and direction. SCIPUFF was originally developed to use observations from nearby Met observing sites, and the model would internally calculate the needed Met profiles using standard BL profile formulas. However, SCIPUFF has been transitioning towards sole use of Met inputs provided in real time by several Met forecast models. These Met model forecasts are accessible to HPAC/SCIPUFF through the Meteorological Data Server (MDS). Currently SCIPUFF uses the Met model outputs of surface heat flux, BL height, and BL profiles of wind speed and direction and temperature. BL profiles of turbulence are simulated by SCIPUFF using the Met models' surface heat flux and momentum flux estimates, coupled with an estimate of the surface roughness length, z_o.

The question naturally arises whether the BL inputs provided by the Met models agree with observations and with the internal parameterizations by SCIPUFF. The Met model outputs and the SCIPUFF simulations of BL variables are compared with observations at several sites in the U.S. Central Plains for three days of extensive experiments in 2002 during the **I**nternational **H**2**O P**roject (IHOP, Weckwerth et al. 2004). The Met models used for the comparisons are the Fifth-Generation Pennsylvania State University / National Center for Atmospheric Research Mesoscale Model (MM5; Dudhia 1991; Grell et al. 1995) and Weather Research and Forecast – Nested Mesoscale Model (WRF-NMM)

Corresponding author address: Steven R. Hanna, Hanna Consultants, 7 Crescent Ave., Kennebunkport, ME 04046-7235, hannaconsult@roadrunner.com

(Janjic, 2003). The current paper provides an overview of the models and their assumptions, reviews the IHOP field experiment, and presents the results of the comparisons. A key question is whether more development is needed before the Met model turbulence outputs can be confidently used by SCIPUFF.

2. THE IHOP FIELD EXPERIMENT

The International H_2O Project (IHOP) took place in the U.S. Southern Great Plains for several weeks from 13 May to 25 June 2002. The field experiment and some highlights were described in a review article by Weckwerth et al. (2004). The fact that "H_2O" is in the name of IHOP is an indication that the primary concern was measurements of water vapor, clouds, and precipitation, and improvements in forecasts of these quantities. Many research organizations took part in IHOP with "a plethora of water vapor measuring systems…to sample the 3D moisture distribution". The goal of the boundary layer heterogeneity (BLH) component of IHOP was to investigate the effects of the surface on BL fluxes and structure (LeMone et al., 2007b). Although the overall goal of IHOP was to further knowledge of atmospheric water vapor and its effects on convection, the BL component focused on case days without significant moist convection in order to better understand surface – BL relationships under simpler, fair weather conditions with the hope that this knowledge could be applied to moist convective cases.

The IHOP data set was chosen for use in the current comparisons because it has an extensive network of sonic anemometer observations of near-surface turbulence and turbulent fluxes, as well as high-resolution balloon sondes or radiosondes every three hours. Another reason is that the research group at Penn State was already analyzing and modeling the IHOP data period (Kang 2007, Kang et al. 2007, Reen 2007). Also, researchers in other groups were intensively analyzing the data and publishing results (e.g., Lemone et al., 2007a and b).

Three days were selected for analysis (29 May, 6 June, and 7 June) because of their use in other IHOP studies and because they were typical of the period, with variable cloudiness, limited rain, and relatively complete data bases. On 29 May there was little daytime rain over most of the study area, and on 6 June and 7 June, there was almost no precipitation over the study region.

Figure 1 and Table 1 contain a map and a listing of names and locations of the 16 IHOP sites used in the current paper. Most of these data were in the IHOP data archive, but some of the turbulence data were separately-provided by IHOP principle investigators (J. Shinn and D. Cook). The Central Facility at Lamont, OK, released radiosondes every three hours, and we analyzed the temperatures, wind speeds and directions, and relative humidity (RH) from that site. In addition, there were sonic anemometers mounted at levels of 4 m and 60 m on a tower at Lamont. The 60 m turbulence data at Lamont were the only IHOP turbulence data available above the near-surface layer from fixed instruments. We note that there were many aircraft flights during IHOP in which turbulence was measured, but we have not included them in this analysis.

Four other sites (Hillsboro, KS, Vici, OK, Morris, OK, and Purcell, OK) took radiosonde and near-surface turbulence data similar to the Central Site at Lamont, but with no sonic anemometer at 60 m. The variations in mixing depth across the five stations will be discussed later, where it is pointed out that a major reason for the differences is the variable cloudiness and rain patterns.

The radiosonde data represent a nearly-instantaneous reading at a given height, and the radiosonde vertical profile is not exactly above the location in Table 1, but is along a slanted trajectory since the balloon is being blown away from its launch site.

Nine sites (numbers 8 through 16) in Table 1 were primarily surface flux sites, where sonic anemometers were located at heights of 2.1 m. In addition, soil heat and moisture fluxes were measured. For IHOP purposes, the fluxes of water vapor and sensible heat were of primary interest. Consequently, we requested other variables such as friction velocity, u*.

The fundamental averaging time for the turbulence observations analyzed here was 30 minutes. The following variables were analyzed:

u^* (m/s) – surface friction velocity (square root of momentum flux divided by air density)

H_s (J/m^{2}s) – Surface sensible (dry air) heat flux

LE (J/m^{2}s) – Surface latent (moisture) heat flux

H_b (J/m^{2}s) – Surface Buoyancy Flux (SBF) (combination of dry air and moisture) flux = H_s + $0.61H_e$

σ_u or (m/s) – Standard deviation of easterly component of turbulent wind speed fluctuations

σ_v (m/s) – Standard deviation of northerly component of turbulent wind speed fluctuations

σ_w (m/s) – Standard deviation of vertical component of turbulent wind speed fluctuations

TKE (m^2/s^2 or J/kg) – Turbulent Kinetic Energy = ½ (σ_u^2 + σ_v^2 + σ_w^2)

u or WS (m/s) – scalar wind speed

WD (°) – Wind direction

T (K) – Temperature

RH – Relative Humidity

Details of IHOP Observations

Several data sets available in the IHOP data archive were investigated for use in this analysis. Because the focus of this study was on atmospheric turbulence, sites with three-dimensional sonic anemometer observations were of special interest, and many of those also included heat and momentum fluxes. Balloon-borne soundings (radiosondes) were operated at five locations providing vertical profile measurements. Each data set is briefly described below.

Balloon-Borne Sounding System (SONDE)

The balloon-borne sounding system, also known as radiosonde or SONDE provides observations of vertical profiles of winds, temperature, pressure and humidity. The SONDE data were obtained from the Atmospheric Radiation Measurement Program (ARM) website at the following location.
http://www.arm.gov/instruments/instrument.php?id=sonde

These systems were operated at five locations during IHOP (Sites 1-5 shown in Table 1). Table 4 lists the SONDE release times at each IHOP location. Balloons were released approximately every 3 hours.

Profiles of temperature and relative humidity were plotted and used to estimate the mixing depth (i.e., PBL height) by eye.

The observed vertical profiles of temperature, wind speed, wind direction and TKE were plotted against the model outputs from MM5 and WRF-NMM and the HPAC assumed profiles for each of the sounding times at each location.

Energy Balance Bowen Ratio (EBBR)

The Energy Balance Bowen Ratio (EBBR) system provides 30 minute averaged estimates of vertical fluxes of sensible and latent heat. These are not observed fluxes but are derived based on observations of net radiation and soil heat flux. If the surface energy fluxes are in balance, the sum of the sensible heat flux and the latent heat fluxes should equal the net radiation flux (to the surface) minus the soil heat flux (away from the surface). By assuming a value for the Bowen Ration, the user can calculate the sensible heat flux and the latent heat flux. However, the accuracy depends on the assumption of an energy balance, the accuracy of the net radiation and soil heat fluxes, and the accuracy of the Bowen Ratio estimate. The estimates of "observed" sensible and latent heat fluxes were available at 3 IHOP EBBP locations (Sites 1, 2, and 4 in Table 1) during the days studied. These data were obtained from the ARM website at the follow location:

http://www.arm.gov/instruments/instrument.php?id=ebbr

The original MM5 and WRF-NMM sensible and latent heat flux outputs for May 29 were compared to the EBBR "observations". Time series plots were created and presented at a meeting in December of 2006. These comparisons raised many questions about the model outputs and ultimately resulted in adjustments being made to both models. Subsequently, it was also decided that the EBBR flux estimates may not be the best to use in our analysis, since they were calculated based on a budget approach as described above.

Eddy Correlation Flux Measurement System (ECOR)

The ECOR system uses fast-response sonic anemometers to provide half-hour measurements of surface turbulent fluxes of momentum, sensible heat and latent heat. These data are available for download from the ARM website for much of the IHOP experiment period. However, none were provided there for these three days. We were able to obtain ECOR data for the Site 1, the C1 - Central Facility, from Ric Cederwall and Marc Fischer at Lawrence Berkeley National Lab. The Central Facility had sonic measurements at two levels, 4 m and 60 m, for May 29, and at one level, 60 m, for June 6 and June 7. The turbulent kinetic energy (TKE) was calculated from the observed ECOR turbulent energy components for comparison with the modeled TKE using the following equation:

$$TKE = \tfrac{1}{2}(uu + vv + ww)$$

The HPAC/SCIPUFF transport and dispersion model makes use of the MM5 or WRF-NMM-simulated surface buoyancy flux, H_b, which is the sum of the sensible heat flux, H, plus 0.61 times the latent heat flux, LE. Consequently the observed surface buoyancy flux SBF was estimated from the ECOR data as:

$$SBF = H + 0.61*LE$$
where,

SBF = Surface Buoyancy Flux
H = Sensible Heat Flux
LE = Latent Heat Flux

ECOR observations were also obtained from two other IHOP sites - Smileyberg, KS and Brainard, KS (Sites 6 and 7 in Table 1). These data were provided to us by David Cook of Argonne National Lab. The sonic anemometers at these sites are at 2.1 m. The Smileyberg site included other meteorological parameters in the data set, such as temperature, relative humidity and wind speed and wind direction at 10m.

The sonic wind speed and wind direction at Smileyberg and Brainard were computed from the horizontal wind components at 2.1 m. Because the

u and v components were shifted 30 degrees in the data archive, the wind direction was adjusted by -30 degree to account for the shift. The same relationships for surface buoyancy flux and TKE that were used for the Central Facility data were applied at Smileyberg and Brainard.

Integrated Surface Flux Facility (ISFF)

The ISFF is managed by EOL/ISF (formerly ATD/RTF) and is designed to study exchanges between the atmosphere and the Earth's surface. There were nine ISFF measurement sites operating during the IHOP Experiment (Sites 8-16 in Table 1). These ISFF locations have both prop (at 10 m) and sonic anemometers (at heights ranging from 2.5 to 5 meters). Table 5 lists the sonic anemometer heights at each site.

Time-averaged statistics of the variables were computed over 5 and 30-minute periods. The turbulence variables are provided in the 5-minute average data sets in the archive. These data were downloaded from the following website location: http://www.eol.ucar.edu/rtf/projects/ihop_2002/isff/

In order to compare the ISFF data with the MM5 and WRF-model outputs and the HPAC/SCIPUFF assumptions, some additional processing of the ISFF data was necessary. The friction velocity ($u*$) and the surface buoyancy flux (H + 0.61LE, or H_b in the data tables) were computed as described below. The sonic wind speed and wind direction were computed from the horizontal wind components, the 10m wind direction was computed from the horizontal wind components, and TKE was calculated from the turbulence variances.

The friction velocity, $u*$, was calculated according to the following equation:

$$u* = (<u'w'>^2 + <v'w'>^2)^{0.25}$$

where the bracket notation ($< >$) denotes an average. The surface buoyancy flux, SBF, was calculated from the ISFF data using the vertical kinematic eddy heat flux, $<w't'>$ (m/s-K) and the vertical kinematic eddy moisture flux, $<w'h2o'>$ (m/s-g/m^3), as follows:

$$SBF (W/m^2) = \rho\, c_p <w't'> + L_v <w'h2o'>$$

where

ρ is the density of air (29/0.0821/T(K) kg/m3),
c_p is the heat capacity of air (1004 J/kg/K) and
L_v is the latent heat of vaporization of water ([2.501 - 0.00237*T(C)]*10^6 J/kg).

3. METEOROLOGICAL (MET) MODELS

The Fifth-Generation Pennsylvania State University / National Center for Atmospheric Research Mesoscale Model (MM5)(Dudhia 1993 and Grell et al. 1995) and Weather Research and Forecast – NonHydrostatic Mesoscale Model (WRF-NMM) (Janjic, 2003) are used in the comparisons with the IHOP data. MM5 is one of the more widely-used models in the U.S., and WRF-NMM is the official forecast model used by the National Centers for Environmental Prediction (NCEP). These models are used as a primary input for HPAC via the Meteorological Data Server (MDS).

3.1 MM5

The MM5 model was set up in the triple nested grid configuration shown in Figure 2. The three nested domains have grid sizes of 36, 12, and 4 km, and each have 62 vertical sigma levels with the model top at 50 mb. The 36 and 12-km domains start 12 h before the start of the case day (12 UTC) and integrate for 36-h while the 4-km domain starts 12 h later (00 UTC) and continues for 24 h. The initial conditions and lateral boundary conditions for the coarse domains were defined using Eta Data Assimilation System (EDAS) analyses enhanced using surface and rawinsonde data by a modified successive scan objective analysis method (Benjamin and Seaman 1985). The EDAS analyses enhanced by observations were also used on the course domains for analysis nudging above the PBL.

For this work, MM5v3.6 is used but with the Noah LSM updated to MM5v3.7.3 and with some alterations. The biggest alteration is that the Gayno-Seaman TKE scheme (Stauffer et al. 1999; Shafran et al. 2000; Stauffer et al. 2001) has been coupled with the Noah LSM here, since the standard version of MM5 does not have this coupling. In the standard version of MM5, Noah is only coupled to other PBL schemes.

MM5 PBL Diagnosis   In the MM5 Gayno-Seaman TKE scheme (Shafran et al. 2000, Stauffer et al. 1999 and 2001), the mixing depth (or PBL height) is estimated as the first layer where the TKE falls below the smaller of a) 0.1 m^{2}s^{-2} and b) half of the maximum TKE in the column. The 0.1 m^{2}s^{-2} criterion works well in situations with strong TKE but was found not to work well in special cases where a mixed layer existed with weak TKE (e.g. stratocumulus layers over the ocean). The "half of the maximum TKE in the column" criterion works well in the special cases and has been found to work reasonably well in some cases over land with stable stratification (e.g., where there's only weak shear-driven turbulence). There are a few exceptions to this methodology:

1. If maximum TKE or TKE at the lowest model level is <0.04 m^{2}s^{-2} then the mixing depth is diagnosed as the first model full layer above the ground (here ~60 m).

2. If in stability regime 1 (stable; bulk Richardson number >= 0.2) then the mixing depth is diagnosed as 0 m. This is not to say there is no mixing depth, but a) with typical MM5 vertical resolution we cannot accurately diagnose

it, b) TKE predictions in GS for stable conditions have not been evaluated sufficiently, and c) it is not clear that model TKE is the best model predictor of mixing depth in stable conditions.

3. If mixing depth diagnosed is greater than 5000 m then it is set to 5000 m. This limits problems when moist convection results in very high mixing depth diagnoses and limits numerical issues that may occur if the mixing depth outside moist convection reaches above this height.

MM5 TKE during stable conditions The Gayno-Seaman (GS) scheme was originally formulated such that during stable conditions (regime 1; diagnosed when Bulk Richardson number >=0.2), a simpler first-order non-TKE PBL methodology known as the Blackadar PBL (Zhang and Anthes 1982) was used. Therefore no TKE was calculated during stable conditions. However, TKE is now calculated in GS for all regimes. During stable conditions the TKE is often smaller than the background value of 0.001 $m^2 s^{-2}$, and so the TKE output defaults to 0.001 $m^2 s^{-2}$. Since the vertical resolutions typical for mesoscale models are too coarse to accurately resolve mixing depth for stable conditions limited attention has been paid in the GS scheme to the performance of the TKE predictions during stable conditions. Thus, there is limited confidence in the TKE predictions from GS during stable conditions. Therefore we recommend not using TKE during stable conditions (Regime 1), especially to determine a reliable mixing depth. It probably makes more sense to consider either a Richardson number approach or as a default, make mixing depth equal to the lowest model half-depth (here ~30 m). The MM5 developers are considering such an approach for implementation into the GS scheme. For all other regimes TKE should be used. Note that the regimes in GS are output as variable "REGIME" and are diagnosed as follows:

Regime 1: Stable conditions (R_b>=0.2)
Regime 2: Damped mechanical turbulent
   Conditions (0.0<R_b<0.2)
Regime 3: Forced convection (R_b<0.0 and
   z_i/L<=1.5)
Regime 4: Free convection (R_b<0.0 and
   z_i/L>1.5)

where

R_b=bulk Richardson number (the temperature difference between the ground and the lowest model layer [here ~30 m AGL] is used in this calculation)

z_i=model-diagnosed mixing depth

L=Monin-Obukhov length

Software to output PBL variables Coding was added to MM5 to output at every time step at selected locations all fields output in the standard output file. Software (TSREAD and TSPLOT) was developed to allow these time series (and similar output from WRF) to be averaged over arbitrary time lengths and plotted.

3.2 WRF-NMM

The WRF-NMM (Non Hydrostatic Mesoscale model) configuration that was used was V2.1.16 (12/19/06 version, Janjic, 2003), employing the expanded CONUS 12 km configuration with 60 sigma pressure hybrid vertical levels The NMM was configured to be as close as possible to the current operational North American Model (NAM) configuration that is run at NCEP 4 times per day.

That configuration was emulated to a large extent with the WRF launcher capability. Therefore, the WRF-NMM was run at 12 km horizontal resolution for much of North America and 60 hybrid sigma-pressure levels. The first model layer is approximately 40 deep. The model physics and dynamics are the same that are run by the operational NAM with Ferrier cloud microphysics, Betts-Miller-Janjic convective parameterization, Mellor-Yamada Janjic (MYJ) TKE based planetary boundary layer parameterization, the NOAH land surface model and GFDL Lacis-Hansen radiation. The model is run on a Rotated latitude longitude grid with Arakawa E grid staggering. Lateral boundary conditions come from the NCEP Global Forecast System (GFS) with initial conditions from the NAM 3-D variational Data Assimilation System (NDAS) as configured during IHOP. The NDAS assimilates surface, radiosondes, profilers winds, Aircraft (ACARS) meteorological data as well as satellite direct radiances from GOES, AVHRR and SBUV satellites. The NOAH land surface model is continuously cycled with observed precipitation from the NWS River Forecast Center (RFC) gridded estimates.

The NMM MYJ PBL scheme (Janjic, 2002) has been the scheme used in the NCEP operational WRF since 2006 and in previous NCEP operational mesoscale model, Eta. In MYJ, the Mellor and Yamada Level 2.5 scheme was modified in order to (i) identify the minimum conditions that enable satisfactory performance of the scheme in the full range of atmospheric forcing, and (ii) develop a robust, consistent, accurate and affordable computational procedure for application in synoptic and meso scale models. In order to achieve the first goal it is sufficient to impose an appropriate upper limit on the master length scale in addition to requiring that the turbulent kinetic energy (TKE) and the master length scale be positive. This upper limit is proportional to the square root of TKE and a function of buoyancy and shear of the driving flow. In the unstable range this function is defined from the requirement that the TKE production be

nonsingular in the case of growing turbulence, and in the stable range the function is derived from the requirement that the ratio of the vertical velocity deviation variance and TKE cannot be smaller than that corresponding to the regime of vanishing turbulence. Thus, within the PBL the master length scale is estimated using the usual diagnostic formula, and above the PBL it is computed as a fraction of the vertical grid size. The values of the master length scale are then modified if necessary in order to satisfy the described constraint.

The TKE production/dissipation differential equation is solved iteratively over a time step. In each iteration, the differential equation obtained by linearizing around the solution from the previous iteration is solved. Two iterations appear to be sufficient for satisfactory accuracy, and the computational cost is minor.

Planetary boundary layer height (i.e., mixing depth) is computed when TKE reaches a critical minimum value of 0.1 m^2s^{-2}. For stable and weak situations when TKE is less than the minimum value at all levels, the PBL height is set to the first model layer depth.

The empirical constants have been revised. However, the techniques and methods of the scheme remain general, in the sense that they can be used with any other reasonably chosen set of constants. The MYJ employs similarity theory to parameterize the surface layer (Janjic, 1996a, b).

The time series software was upgraded to WRF V2.1.16 and the three IHOP case days were run. The North American Model (NAM) WRF initial and boundary conditions and 48 hour runs were made. Tables of time series outputs were provided at 16 IHOP observation sites for further analysis of various boundary layer fields. The predicted fields were plotted using the Penn State University TS utilities. These predicted boundary layer fields are also plotted at:

http://www.emc.ncep.noaa.gov/mmb/mt/misc/html/2002052812/ts16.html

Figure 3 shows the WRF-NMM domain. Further details of the WRF runs are: i) initialized atmospheric states with WRF SI/REAL from EDAS/Eta forecasts; ii) initialized land surface with Gayno-Gridgen utility from original EDAS land states (but continue to use new WRF land states); iii) EDAS soil moisture scaled to current new operational 24 class soil types in WRF-NMM; and iv) model Domain: expanded CONUS (1.6x smaller than full NAM domain), with model top at 50 mb.

4. HPAC/SCIPUFF METEOROLOGICAL "DATA" USED IN COMPARISONS

Given a set of MM5 or WRF outputs for the IHOP periods, the first step was to use standard software to convert them to the so-called MEDOC format for direct use by HPAC/SCIPUFF. In the current paper, only the MM5 outputs were converted to MEDOC format, since the WRF

conversion was not yet available. The MEDOC file includes boundary layer variables such as mixing depth, surface buoyancy flux, and vertical profiles of wind speed, wind direction and profiles. Surface roughness files were also obtained from MM5. HPAC/SCIPUFF uses the MEDOC outputs at each grid location, combined with standard boundary layer profile formulas, to calculate vertical profiles of turbulent speed components (σ_u, σ_v, and σ_w) and Lagrangian time scales.

For comparison with the Met model outputs and the IHOP observations, we needed to extract meteorological profiles from the HPAC/SCIPUFF simulations. Surface roughness, z_o, was varied in space, as done in MM5. Default HPAC settings were used for all other input variables. To extract profiles, the keyword MET TURB was used to "sample" the meteorology being used within HPAC.

5. METHODS USED FOR COMPARISONS

The MM5 and WRF-NMM model simulations, the HPAC/SCIPUFF parameterizations, and the observed Met variables were compared. We note that there is somewhat of a mismatch in the effective averaging times and distances in this comparison. The Met model (MM5 and WRF-NMM) simulations represent an average over a three dimensional grid, with thickness about 50 or 60 m next to the ground and horizontal grid size of 4 km for MM5 and 12 km for WRF-NMM. The model simulations at small time steps are combined to form 30 min time averages. In contrast, the sonic anemometer observations, averaged over the same 30 min period, represent a single point within the much larger model grid volume. Clearly the point observation will have more variability than the volume average. To compare the observations with the model simulations in an ideal consistent manner, there would have to be thousands of sonic anemometers within the grid volume and all would be averaged. Of course this is economically infeasible.

Another cause for a mismatch is that the model simulation represents a "subgrid" value, and it is assumed that grid-to-grid variability (at larger scales) is resolved by the model. In contrast, the turbulence measured by the single sonic anemometer is sampling from all scales of motion.

Researchers have attempted to make the point observations more representative of a smoothed grid average by employing statistical methods such as kriging. Then the kriged observations are compared with the grid-volume averaged simulations by the model. But this method has been criticized because the kriging method represents another model and therefore you are comparing one model with another.

The TKE comparison also has issues, because the Met models simulate only the total TKE and do not break it down into components (σ_u, σ_v, and σ_w). But any dispersion model (e.g., HPAC/SCIPUFF)

needs the components to calculate the rate of dispersion in the three directions. SCIPUFF also needs the scales of turbulence in the three directions. Thus we can compare the observed, Met model simulated, and SCIPUFF parameterized TKE but not the σ_u, σ_v, and σ_w. If the Met model-simulated TKE is to be used in SCIPUFF (or any other dispersion model), it is necessary to be able to partition the TKE into σ_u, σ_v, and σ_w. This can be done using similarity theory, as used in SCIPUFF, but further testing is needed.

With these caveats, we have proceeded with the following comparisons

- Mixing depths (i.e., PBL height) are output by MM5 and WRF-NMM, and are compared with those estimated by eye from the radiosonde T and RH profiles, taken every 3 hours.
- Profiles are available from MM5 and WRF-NMM in the boundary layer at height increments of about 50 to 100 m. The simulated variables u (wind speed), WD (wind direction), and T are compared with the observed radiosonde profiles of these variables. The HPAC/SCIPUFF profiles of these variables are also compared, although it is expected that the modeled profiles would be identical to the Met model simulations. We did find a bias in temperature in the SCIPUFF temperature profiles, and found that it was caused by a typo in the potential temperature conversion equation. This was subsequently corrected.
- Profiles are presented at a full boundary layer scale from z = 0.0 to 3000 m, and also at a zoomed-in scale of 0.0 to 300 m near the surface. During stable conditions, there are often shallow inversions that are seen better in the zoomed-in plots.
- Met model simulated profiles of TKE were compared with HPAC/SCIPUFF parameterizations of TKE. SCIPUFF uses Met model simulations of mixing depth, surface buoyancy flux, u*, and an input of z_o to make these calculations. The only observations of TKE were made at z = 2 or 4 m at all sites except the Central (Lamont, OK) site, where an observations was also available at z = 60 m.
- MM5 and WRF outputs of surface sensible and latent heat fluxes, buoyancy flux, and u* were compared with near-surface observations at all 16 sites.
- Met model simulated time series of mixing depth (PBL height), surface fluxes, and vertical profiles of wind speed and direction, temperature, and turbulence (TKE) are compared with observed time series.

MM5 and WRF-NMM model outputs were provided in a time series format. The TSREAD and TSPLOT software was developed to time-average the time series outputs and extract and plot the various parameters. (A more complete description of the software and the MM5 and WRF-NMM model outputs are provided in Appendix A). Model outputs were averaged in 5-minute and 30-minute blocks. The 5-minute averages were used in profile comparisons and in the time series comparisons with the ISFF observations. The 30-minute averages were used in the time series comparisons at sites 1, 6, and 7 (Central Facility, Smileyberg and Brainard).

The HPAC/SCIPUFF transport and dispersion model accepts inputs from MM5 and WRF-NMM. It directly uses the mixing depths, the wind and temperature values at the Met model levels, and the surface buoyancy flux (SBF). HPAC/SCIPUFF interpolates the wind and temperature profiles to other levels. It uses the surface fluxes and the mixing depth, along with an estimate of the surface roughness, z_o, to parameterize values of TKE at various levels. Actually, HPAC/SCIPUFF parameterizes the components of TKE (uu, vv, and ww). Appendix B describes the formulas and assumptions used in these parameterizations.

The observed TKE was calculated from the observed turbulent components in the x, y, and z directions for comparison with the modeled TKE. The following equation was used:

TKE = ½*(uu + vv + ww)

where

uu is the u variance of horizontal wind
vv is the v variance of horizontal wind
ww is the w variance of vertical wind

Golden Software GRAPHER7 was used to generate the plots. Vertical profile plots were generated for May 29th, June 6th and June 7th for the following locations: Central Facility, B1, B4, B5, and B6. The vertical profile plots contained HPAC parameterizations, MM5 output, WRF-NMM output and when available, observed data. The following variables were plotted: temperature with mixing heights indicated, wind direction, wind speed and turbulent kinetic energy.

Time series plots were generated for May 29th, June 6th and June 7th for sites 1, 6, and 7 (the Central Facility, Smileyberg and Brainard) and the nine ISFF sites showing HPAC, WRF, MM5 and observed data. The MM5 and WRF-NMM wind speeds were adjusted using a logarithmic profile to estimate the wind speed at the observed height. Other variables were not extrapolated or interpolated and the height of the data is shown on the plot. The formula used to extrapolate the wind speed is:

$$u(zobs) = u(zmod) \; (\ln(zobs/z_o)/\ln(zmod/z_o))$$

where

zobs is the observation height

zmod is the model height

z_o is the surface roughness length

5. COMPARISONS OF VERTICAL PROFILES

There were about 720 profile plots generated (three days with 8 profiles per day at five locations and six variables). A few representative plots are presented and discussed in this paper.

5.1 Characteristics of Observed Temperature and RH Profiles

Mixing depths were estimated by eye for each radiosonde profile. The "textbook" shapes for vertical temperature and RH profiles were found to not always occur in reality. Figure 4 is an example of a textbook set of daytime temperature and RH profiles, with a superadiabatic layer near the ground, an adiabatic layer from 50 m to 1070 m, and a sharp 2 C capping inversion from 1070 m to 1100 m. The RH profile shows a sharp drop (from 67 % to 40 %) at 1070 m. Thus the analyst can say with much confidence that the mixing depth (or PBL height) is 1070 m. However, Figure 5 is an example of a situation where the mixing depth is not so obvious, with no sharp capping inversion or RH drop. Because of the fact that RH is near 100 % in the layer from 1100 m to 1500 m, it is likely that clouds were present, and this was confirmed by the satellite data and the local weather observations. Other scenarios that can lead to an uncertain mixing depth are i) multiple capping inversions due to advection from upwind areas, ii) residual layers and capping inversions from previous hours, and iii) variable cloudiness and/or other phenomena that cause time and space variations in the BL.

Stable conditions present a challenge when mixing depth must be estimated. Intuitively, the mixing depth marks the top of the layer near the ground where there is significant vertical mixing, but the radiosondes do not measure TKE or other indications of mixing. The mixing depth is not the top of the surface inversion layer. Thus, the mixing depth can be determined during stable conditions only for weakly-stable nearly-neutral periods, when there is a capping inversion and/or RH drop evident.

5.2 Comparison of Observed and Simulated Vertical Temperature Profiles and Mixing Depths

The challenges in interpreting mixing depths from the observed profiles were reviewed in the previous subsection. In this subsection, examples of plots are presented where the observed, MM5,

WRF-NMM, and HPAC/SCIPUFF temperature profiles are shown, as well as indications of mixing depth. Both MM5 and WRF-NMM determine the mixing height as the level where the TKE first drops below some arbitrary minimum value. This assumed minimum TKE has been set based on a combination of scientific reasoning and calibration with many observed data. The WRF-NMM developers are currently planning to increase their minimum TKE assumption for mixing depth, because of accumulating evidence that the mixing depth is being overestimated (see Figure 6).

Figure 6 compares the observed and simulated temperature profiles and mixing depths, for the Lamont, OK, Central Facility site for 2030 UTC (1530 LDT) on 29 May 2002. This is a "textbook" profile with a clear capping inversion and observed mixing depth of 1310 m. Note that the MM5 and HPAC profiles and mixing depths are nearly identical since the MM5 outputs are directly used by HPAC. It is seen that the MM5 and WRF-NMM profiles are similar to the observed profiles, although both have the capping inversion at heights about 150 m lower than the observed. MM5's estimated mixing depth is close to the base of its simulated capping inversion, at 1190 m, about 120 m less than the observed value. WRF-NMM's mixing depth estimate is about 1680 m, which is about 460 m higher than its own capping inversion base, and is about 370 m larger than the observed. This trend is seen in most of the radiosonde profiles.

Figure 7 is the same type of plot as Figure 6, except for a stable period (0841 UTC or 0341 LDT at Lamont OK on 29 May 2002). Figure 8 zooms in on the lower part of the profile in Figure 7, so that the details of the surface-based inversion can be seen.

The observed profile has a 3.5 C surface inversion in the lowest 100 m, with a variable profile, between adiabatic and isothermal, above that. WRF-NMM simulates the surface inversion. MM5 has a near-adiabatic layer near the surface in this profile, but an inversion does form in later MM5 profiles (not shown here). WRF-NMM simulates the observed deep layer with a gradient between adiabatic and isothermal, but MM5 has a 5 C capping inversion between 800 and 1100 m. The simulated mixing depths are all less than 100 m, but have considerable variability. No observed mixing depth is indicated in Figure 7 because of the surface based inversion. However, observed (20 m) and simulated (40 m for HPAC and 70 m for WRF-NMM) mixing depths are shown on Figure 8.

5.3 Comparisons of Observed and Simulated Vertical Profiles of Winds and TKE

The wind speed comparisons generally indicate variability. The observed winds themselves were variable in space and time over the domain, because of the frequent presence of fronts, clouds

and rain, and mesoscale phenomena (which were one of the main focuses of IHOP). The Met model simulated winds were also variable, and it was possible to have disagreements with observations even though the Met model successfully simulated the formation of a cloud area or a front. This is because the Met model timing might be a few hours off in the frontal passage or might displace the center of a small wave by 200 km.

Figure 9 shows profiles of wind speed for Lamont, OK, at 2030 UTC (1530 LDT) on 29 May. This is the same location and time used for the temperature profile comparison in Figure 6. Note that the observed winds are about 3 m/s in the 100 m layer near the surface and gradually decrease to about 1.2 m/s at a height of 800 m. The WRF-NMM simulated winds are nearly uniform with height, but at about 5 m/s (i.e., 2 to 3 m/s greater than the observed). The MM5 simulated winds, on the other hand, are light (less than 1 m/s) in the lowest 200 m and slowly increase to 2 m/s at z = 800 m. If the HPAC/SCIPUFF model were to simulate a pollutant release near the ground, the effective cloud speed would be much different depending on which wind speeds were used – the observed, the MM5, or the WRF-NMM.

The TKE profile comparisons are of special interest because of the desire to incorporate Met model TKE outputs as inputs to HPAC/SCIPUFF. As stated earlier, the Lamont, OK, central site was the only one with an observed profile of TKE, at heights of 4 and 60 m. Figure 10 shows the observed, the HPAC-parameterized, and the MM5 and WRF-NMM-simulated TKE profiles for the same time as Figures 6 and 9. There is good agreement (given the typical variability) seen in Figure 10. Observed TKE is 1.3 and 1.5 J/kg (m^2/s^2) at heights of 4 and 60 m, respectively. The MM5 and the WRF-NMM-simulated TKE is about 30 % smaller than the observations. The HPAC-parameterized TKE is about 20 % larger than the observations. The HPAC TKE is always about 0.7 J/kg larger than the MM5 value. This is about 50 % larger at heights of 200 to 700 m, but is a factor of three or more larger at heights above 1000 m and approaching the mixing depth.

6. COMPARISONS OF TIME SERIES

There are about 216 time series plots (three days for 12 sites for six variables). A few examples are described below.

6.1 Comparisons of T, WD, WS, u*, TKE, and SBF for the Central Facility Site for the Three Days

This section presents the time series for one site, the Central Facility in Lamont, OK, for all three days and for six variables (T, WD, WS, u*, TKE, and SBF. Figures 11-16 contain these time series plots, with one variable and three days per page.

As before, the observations, the MM5 and WRF-NMM simulations, and the HPAC parameterizations are shown in each time series.

The T plots in Figure 11 show that the models are simulating too low temperatures, by about 4 C, during the nights of 29 May and 7 June. There is good agreement during the night of 6 June. The model T predictions during the day are closer to the observations.

The WD plots in Figure 12 show more variability in predictions on 29 May and 6 June, although some of the fluctuations are due to the WD frequently passing through N and having a 0 degree to 360 degree discontinuity. This discontinuity is an artifact of the plotting method. Best agreement (within about ± 20°) is seen during the daytime on 6 June and all day on 7 June. On 7 June, there were SE winds all day at moderate strength.

The WS comparisons in Figure 13 suggest an RMSE difference of about 2 or more m/s on 29 May and 6 June, with large biases during a few periods. For example, the observed WS is about 1 to 2 m/s most of 29 May. But MM5 predicts 4 m/s during the night and calm during the day. WRF-NMM tends to overpredict all day on 29 May. As with the WD plots, the best agreement is seen on 7 June.

The u* time series in Figure 14 are puzzling since the HPAC parameterized values are generally much too high (by more than a factor of two) at night. One reason why this is puzzling is that the WS differences were not as great and u* is roughly proportional to WS. In fact the HPAC u* values are nearly constant day and night, in contrast to the shape of the observed and Met model-simulated curves. However, the daytime HPAC parameterized u* values are generally roughly equal to the observations. The MM5-simulated u* tends to be high by 50% to a factor of 2.

Figure 15 shows the TKE time series. The agreement between the models and the observations is better during the daytime, when there is a large increase beginning at sunrise and peaking at about 1500, and decreasing again towards sunset. The met models tend to underpredict the afternoon TKE values by about 30 or 40 %. The HPAC parameterized curve matches the daytime observations fairly well (including near sunrise and sunset). During the night, the HPAC parameterized TKE values tend to be about a factor of two to five larger than the observed values. There is no MM5 TKE prediction at night because of the very stable BL regime being used in its closure scheme. The WRF-NMM predicted TKE at night is seen to be at its minimum value, 0.1 J/kg (m^2/s^2), most of the time. This happens to be fairly close to the observed TKEs.

The surface buoyancy flux (SBF) is plotted in Figure 16. During the night, the observed and simulated values are all very close to 0.0. This was unexpected, because most nighttime SBFs elsewhere have fluxes of about – 20 to -50 J/kg

(W/m^2) occurring quite frequently. It may be that the sensible heat flux and latent heat flux are cancelling each other out at this location on these days. The simulated daytime SBFs match the observations quite well, on average.

6.2 Comparisons of TKE for 12 Sites for the Three Days

The TKE outputs and observations are of most interest to the current study. There is one TKE time series plot in Figures 17a through 17l for each of the 12 sites (CF1, Smileyberg, Brainard, and ISFF 1 through 9, respectively) with a TKE observation. All plots are for June 7, which was marked by moderate winds from the southeast and no precipitation.

The difference in the TKE curves as observed and as simulated by MM5 and WRF-NMM between day and night is very evident. During the night, these three curves show low TKE values of about 0.1 to 0.3 J/kg (m^2/s^2). During the day, TKE increases dramatically and a clear "hump" is seen, with a maximum of 1 to 3 J/kg (m^2/s^2) at about 1200 minutes UTC, or about 2000 hr UTC or about 1500 hr LDT. The hump looks like the positive part of a cosine curve and decreases to nighttime values at about sunrise and sunset.

During the day, the two models and the HPAC parameterizations are within a factor of two of the observed curve. There is a variability from site to site, though. MM5 and WRF-NMM are low by about 20 % or so on average during the day. MM5 appears to nearly always predict larger TKE than WRF-NMM during the day.

During the night, the HPAC parameterized TKE has very large overestimates (up to a factor of 10 to 20) at 9 of the 12 sites. The 9 sites all have low observed TKE (about 0,1 J/kg). The three sites with better agreement between the HPAC parameterizations and the observations have relatively high nighttime TKE

7. CONCLUSIONS

The IHOP balloon sounding profile observations in the BL and the surface flux and turbulence observations have been compared with outputs of the MM5 and WRF-NMM Met models and with the parameterizations by the HPAC/SCIPUFF dispersion model. Three days have been studied – 29 May, 6 June, and 7 June 2002.

There is general interest in how well the Met model simulations/outputs agree with BL observations. But the primary interest is whether the Met models TKE outputs are of sufficient accuracy to incorporate as inputs to HPAC/SCIPUFF.

The current paper presents figures showing the qualitative degree of agreement for many of the observing sites and time periods and variables. Future papers will incorporate comprehensive quantitative statistics (e.g., RMSE in WS over all near-surface IHOP observation sites and days).

The following conclusions are seen in the balloon-soundings:
i) Clear observed mixing depths (PBL heights) are seen in only about ½ of the soundings during the day. The MM5 mixing depths match the observed values within about ±20 to 40% and have little mean bias. The WRF-NMM mixing depths have similar scatter but are too high by about 30 % on average.
ii) At night, the observed mixing depths are often shallow (e.g. 20 m) and the resolutions of the Met models are insufficient to detect these shallow layers.
iii) The Met models simulated WS profiles in the BL (up to about 1000 m) seldom match the observations and often have large biases. The large biases are generally due to slight misplacement of fronts or waves in time and space. After the mean bias is removed, the scatter is still about 1 to 3 m/s.
iv) The Met models TKE profiles have generally better agreement during the day, when there is not much variation of TKE with height.
The following conclusions are seen in the time series plots near the surface at the Central Facility (Lamont, OK) for the three days:
i) The Met models usually (but not always) underpredict the nighttime T by a few degrees. Agreement is better during the day.
ii) The nighttime WDs tend to be variable and lead to large Met model RMSE values. 7 June is an exception, with steady SE observed and simulated WDs, and agreement of about ±20 degrees. The daytime WDs have better agreement (±20 degrees most of the time)
iii) The simulated WS has an RMSE of about 2 m/s and sometimes large mean biases (e.g., 29 May for MM5, which underpredicts by a large amount).
iv) The Met models u* simulations tend to track the observations with typical scatter of less than a factor of two. However, the HPAC u* parameterization is much too large at night.
v) The Met models TKE simulations are fairly good (within about a factor of two) during the daytime, but tend to underpredict the mid-afternoon maximum by about 30 to 40 %. The HPAC/SCIPUFF parameterized TKE has two curves – the solid line uncorrected for averaging time and the dashed curve corrected for averaging time. The latter, which is stated to be the preferred curve, has a slight underprediction trend during the day. Like u*, TKE is greatly overpredicted (by a factor of two to five) by HPAC/SCIPUFF at night.
vi) The surface buoyancy flux (SBF) is close to zero at night for the observations and the Met models and for HPAC. During the day, the models match the general cosine curve of SBF,

although the scatter is about ±20 to 40% for the comparison of the 30-min averages.

The following conclusions are seen in the time series plots near the surface for TKE at the 12 sonic anemometer sites for all three days:

i) During the day, the Met model simulations and the HPAC parameterizations of TKE are usually within a factor of two of the observations. On average, the MM5 and WRF-NMM simulations are low by about 20%. The HPAC TKE value corrected for the 30-minute average is 20 % to a factor of two less than the original uncorrected value.

ii) During the night, the observed TKE value is much smaller than during the day and the WRF-NMM model simulations are within a factor of two much of the time. The MM5 TKE outputs are often not available at night because of its BL closure scheme. The HPAC parameterized TKE is usually much too large, by a factor of 10 to 20.

Some recommendations for the future are: 1) Develop the optimum way to incorporate Met model TKE outputs in HPAC/SCIPUFF, and 2) Recommend possible Met model modifications based on comparisons of Met model BL profiles with observations. Note that it will also be necessary to partition the Met model simulated TKE into the three components, for use in HPAC/SCIPUFF (or any dispersion model).

ACKNOWLEDGEMENTS

REFERENCES

Benjamin, S.G. and N.L. Seaman, 1985: A simple scheme for objective analyses in curved flow. *Mon. Wea. Rev*., **113**, 1184-1198.

Chen, F., K.W. Manning, M.A. LeMone, S.B. Trier, J.G. Alfieri, R. Roberts, M. Tewari, D. Niyogi, T.W. Horst, S.P. Onley, J.B. Basara, P.D. Blanken, 2007: Description and evaluation of the characteristics of the NCAR High-Resoluation Land Data Assimilation System. *J. Appl. Meteor. Clim*., **46**, 694-713.

Cox, R., B.L. Bauer and T. Smith, 1998: A mesoscale model intercomparison. *Bull. Am. Meteorol. Soc*., **79**, 265-283.

Cullen, A.C. and H.C. Frey, 1999: *Probabilistic Techniques in Exposure Assessment. A Handbook for Dealing with Variability and Uncertainty in Models and Inputs*. Plenum Press, New York, 335 pp.

Dabberdt, W.F. and E. Miller, 2000: Uncertainty, ensembles, and air quality dispersion modeling: Applications and challenges. *Atmos. Environ*., **34**, 4667-4673.

DoD (U.S. Department of Defense), 2000: Technical Report - Modeling and Risk Characterization of US Demolition Operations at the Khamisiyah Pit. Special Assistant to the Under Secretary of Defense (Personnel and Readiness) for Gulf War Illnesses, Medical Readiness, and Military Deployments, U.S. Department of Defense, 193 pages. Available from http://www.gulflink.osd.mil/khamisiyah_tech/.

DTRA, 2004: HPAC Version 4.04.011 (DVD containing model and accompanying data and document files). Available from DTRA, Ft. Belvoir, VA.

Dudhia, J., 1993: A nonhydrostatic version of the Penn State/NCAR mesoscale model: Validation tests and simulation of an Atlantic cyclone and cold front. *Mon. Wea. Rev*., **121**, 1493-1513.

Grell, G. A., J. Dudhia, and D. R. Stauffer, 1995: A Description of the Fifth-Generation Penn State / NCAR Mesoscale Model (MM5), NCAR/TN-398+STR, National Center for Atmospheric Research, Boulder, CO, 122 pp.

Hanna, S.R. and R. Yang, 2001: Evaluations of mesoscale model predictions of near-surface winds, temperature gradients, and mixing depths. *J Appl Meteorol.,* **40**, 1095-1104.

Hanna, S.R., R. Yang and X. Yin, 2000: Evaluations of Numerical Weather Prediction (NWP) models from the point of view of inputs required by atmospheric dispersion models. *Int. J. Environ.. and Poll.,* **14**, 98-105.

Hanna, S.R., 1994: Mesoscale meteorological model evaluation techniques, with emphasis on needs of air quality models. In: Pearce R, Pielke R, eds. Chapter in Aspects of Mesoscale Modeling. Meteorological Monographs Series No. 47, AMS, 45 Beacon Street, Boston.

Hanna, S.R., Z. Lu, H.C. Frey, N. Wheeler, J. Vukovich, S. Arumachalam and M. Fernau, 2001: Uncertainties in predicted ozone concentration due to input uncertainties for the UAM-V photochemical grid model applied to the July 1995 OTAG domain. *Atmos. Environ*., **35**, 891-903.

Janjic, Z.I., 1996: The Mellor-Yamada level 2.5 scheme in the NCEP Eta Model. 11th Conference on Numerical Weather Prediction, Norfolk, VA, 19-

23 August 1996; American Meteorological Society, Boston, MA, 333-334.

Janjic, Z.I., 1996: The Surface Layer in the NCEP Eta Model. 11th Conf. on NWP, Norfolk, VA, American Meteorological Society, 354–355.

Janjic, Z.I., 2002: Nonsingular implementation of the Mellor-Yamada Level 2.5 scheme in the NCEP Meso model. NCEP Office Note No. 437, 61 pp.

Janjic, Z.I., 2003: A nonhydrostatic model based on a new approach. *Meteorol. and Atmosph. Phys.* **82**, 271-285. (Online: http://dx.doi.org/10.1007/s00703-001-0587-6).

Kang, S.-L., 2007: The Effects of Mesoscale Surface Heterogeneity on the Fair-Weather Convective Atmospheric Boundary Layer. Ph.D. Dissertation. Pennsylvania State University, 200 pp. [Available from the Dept. of Meteorology, The Pennsylvania State University, University Park, PA 16802]

Kang, S.-L., K.J. Davis and M. LeMone, 2007: Observations of ABL structures over a heterogeneous land surface during IHOP-2002. *J. Hydrometeor.*, **8**, 221-244.

LeMone, M.A., F. Chen, J.G. Alfieri, R.H. Cuenca, Y. Hagimoto, P. Blanken, D. Niyogi, S. Kang, K. Davis, and R. L. Grossman, 2007a: *Bull. Amer. Meteo. Soc..* **88**, 65-81.

LeMone, M.A., F. Chen, J.G. Alfieri, M. Tewari, B. Geerts, Q. Miao, R. L. Grossman, and R.L. Coulter, 2007b: Influence of land cover and soil moisture on the horizontal distribution of sensible and latent heat fluxes in Southeast Kansas during IHOP-2002 and CASES-97. *J. Hydrometeor.*, **8**, 68-87.

Lewellen, W.S. and R.I. Sykes, 1989: Meteorological data needs for modeling air quality uncertainties. *J. Atmos. Oceanic Tech.*, **6**, 759-768.

Pasquill, F.A., 1974: *Atmospheric Diffusion* (2nd ed). Halstead Press, Wiley, New York.

Pielke, R.A. Sr. and M. Uliasz, 1997: Use of meteorological models as input to regional and mesoscale air quality models – limitations and strengths. *Atmos. Environ.*

Pielke, R.A. Sr., 1998: The need to assess uncertainty in air quality evaluations. *Atmos. Environ.*, **32,** 1467-1468.

Reen, Brian P., 2007: Data Assimilation Strategies and Land-Surface Heterogeneity Effects in the Planetary Boundary Layer. Ph.D. Dissertation. Pennsylvania State University, 246 pp. [Available

from the Dept. of Meteorology, The Pennsylvania State University, University Park, PA 16802]

Seaman, N.L., 2000: Meteorological modeling for air quality assessments. *Atmos. Environ.*, **34**, 2231-2259.

Seaman, N.L., D.R. Stauffer and A.L. Lario-Gibbs, 1995: A multi-scale four-dimensional data assimilation system applied to the San Jouquin Valley during SARMAP. Part I: Modeling design and basic performance characteristics. *J. Appl. Meteorol.*, **34**, 1739-1761.

Shafran, P.C., N.L. Seaman, and G.A. Gayno, 2000: Evaluation of numerical predictions of boundary layer structure during the Lake Michigan Ozone Study. *J. Appl. Meteor.*, **39**, 412-426.

Stauffer, D.R., R.C. Muñoz and N.L. Seaman, 1999: In-Cloud Turbulence and Explicit Microphysics in the MM5, 9th PSU/NCAR MM5 Modeling System Users' Workshop, NCAR, Boulder, CO, pp. 177-180.

Stauffer, D.R., R.C. Muñoz, and N.L. Seaman, 2001: On the importance of saturation effects in the turbulence scheme of a mesoscale model. 9th AMS Conf. on Mesoscale Proc., Ft. Lauderdale, FL, 30 July – 2 August, pp. 1-5.

Sykes, R.I. et al., 2003: *SCIPUFF Version 1.6 Technical Documentation.* ARAP report No. 726, Titan Corp., ARAP Group, POB 2229, Princeton, NJ 08543-229.

Sykes, R. I. and R. S. Gabruk 1997: A second-order closure model for the effect of averaging time on turbulent plume dispersion. *J. Appl. Met.,* 36, 165-184.

Sykes, R.I., W.S. Lewellen and S.F. Parker, 1984: A turbulent transport model for concentration fluctuations and fluxes. *J. Fluid Mech.*, **139**, 193-218.

Sykes, R.I., W.S. Lewellen, S.F. Parker and D.S. Henn, 1988: A hierarchy of dynamic plume models incorporating uncertainty. Vol. 4, Second-Order Closure Integrated Puff, EPRI EA-6095, 99 pages, available from ARAP/Titan, POB 229, Princeton, NJ 08543-2229.

Weckwerth, T.M. et al., 2004: An overview of the International H2O Project (IHOP-2002) and some preliminary highlights. *Bull. Amer. Meteorol. Soc.*, **85**, 253-277.

White, J.M., J.F. Bowers and S.R. Hanna, 2007: Importance of using observations of mixing depths in order to avoid large errors by a transport and

dispersion model, submitted to *J. Atmos. and Oceanic Technol.*

Zhang, D., and R.A. Anthes, 1982: A high-resolution model of the Planetary Boundary Layer—Sensitivity tests and comparisons with SESAME-79 data. *J. Appl. Meteor.*, **21**, 1594-1607.

Table 1. IHOP Sites in Kansas and Oklahoma that Are Analyzed in this Paper. Figure 1 Shows the Sites on a Map of the Area. ISFF = Integrated Surface Flux Facility, EBBR = Energy Balance Bowen Ratio, ECOR = Eddy CORrelation Flux Measurement System. The Acronyms LLNL and ANL Refer to Lawrence Livermore National Lab and Argonne National Lab, who Provided Those Data.

Site Num	Site Name	Lat (deg)	Lon (deg)	MM5 Sfc Rough z_o (m)	MM5 elev (m)	Radio Sonde	Sonic anem	EBBR	ECOR
1	C1 - Central Facility – Lamont, OK	+36.605	-97.485	0.15	311	X	X	X	LLNL
2	BF1 - Hillsboro, KS	+38.305	-97.301	0.15	457	X		X	
3	BF4 – Vici, OK	+36.071	-99.204	0.12	628	X			
4	BF5 – Morris, OK	+35.688	-95.856	0.15	214	X		X	
5	BF6 – Purcell, OK	+34.985	-97.522	0.15	348	X			
6	Smileyberg, KS	+37.521	-96.855	0.12	410		X		ANL
7	Brainard, KS	+37.960	-97.102	0.15	421		X		ANL
8	ISFF1	+36.473	-100.62	0.12	875		X		
9	ISFF2	+36.622	-100.63	0.14	846		X		
10	ISFF3	+36.861	-100.60	0.12	784		X		
11	ISFF4	+37.358	-98.245	0.12	500		X		
12	ISFF5	+37.378	-98.164	0.15	493		X		
13	ISFF6	+37.354	-97.653	0.15	406		X		
14	ISFF7	+37.313	-96.939	0.12	366		X		
15	ISFF8	+37.407	-96.766	0.12	427		X		
16	ISFF9	+37.410	-96.567	0.12	431		X		

Table 2. Sonic Anemometer Heights at ISFF Sites

Site in Table 1	ISSF Site	Sonic Anemometer Height (m)
8	ISFF1	2.5
9	ISFF2	3.4
10	ISFF3	2.7
11	ISFF4	2.6
12	ISFF5	5.0
13	ISFF6	4.9
14	ISFF7	2.7
15	ISFF8	4.6
16	ISFF9	4.7

Table 3. Balloon-Borne Sounding Times (UTC; note that LCT = UTC – 5 hrs)

	Site 1	Site 2	Site 3	Site 4	Site 5
	C1	B1	B4	B5	B6
	Central Facility Lamont, OK	Hillsboro, KS	Vici, OK	Morris, OK	Purcell, OK
5/29/02	02:30	02:30	02:29	02:30	---
	05:29	05:30	05:29	05:30	---
	08:41	08:30	---	08:30	---
	11:24	11:36	11:29	11:30	---
	14:28	14:30	14:31	14:30	---
	17:37	17:30	17:29	17:30	---
	20:30	20:30	20:29	20:30	---
	23:33	23:32	23:30	23:30	23:30
6/6/02	02:29	02:30	02:30	02:30	02:30
	05:26	05:30	05:29	05:30	05:30
	08:26	08:30	08:29	08:30	08:30
	---	08:59	---	---	---
	11:33	11:30	11:29	11:30	11:30
	14:27	14:30	14:30	14:30	14:30
	17:28	17:30	17:30	17:30	17:30
	20:33	20:30	20:30	20:30	20:30
	23:30	23:30	23:30	23:30	23:30
6/7/02	02:29	02:30	02:30	02:30	02:30
	05:27	05:30	05:30	05:30	05:30
	08:28	08:30	08:29	08:30	08:30
	11:31	11:30	11:30	11:30	11:30
	14:29	14:30	14:30	14:51	14:30
	17:29	17:30	17:28	17:30	17:30
	20:29	20:30	20:27	20:30	20:30
	23:30	23:30	23:30	23:30	23:30
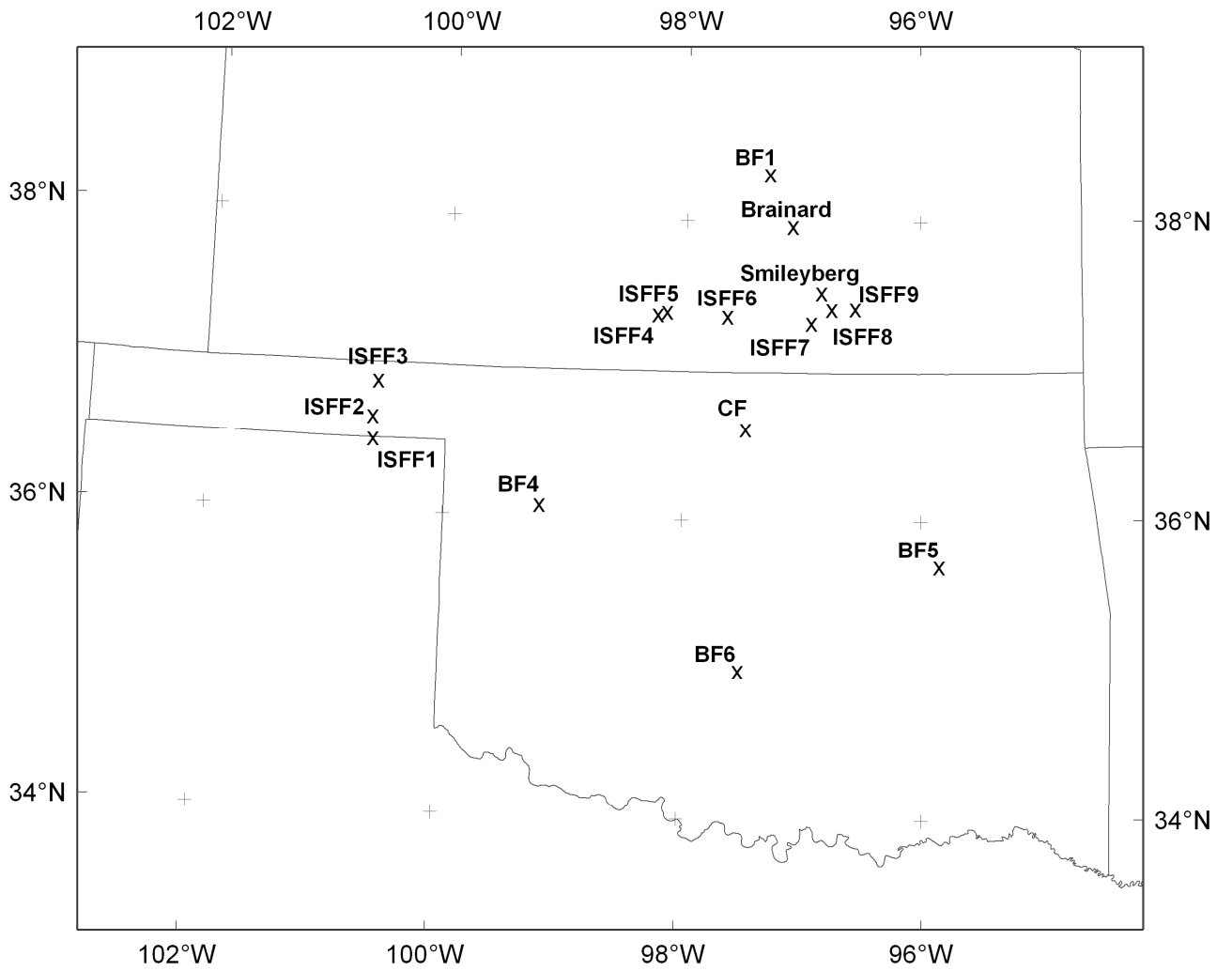
Figure 1. IHOP observing sites used for comparisons in this paper. See Table 1 for details of the site locations.
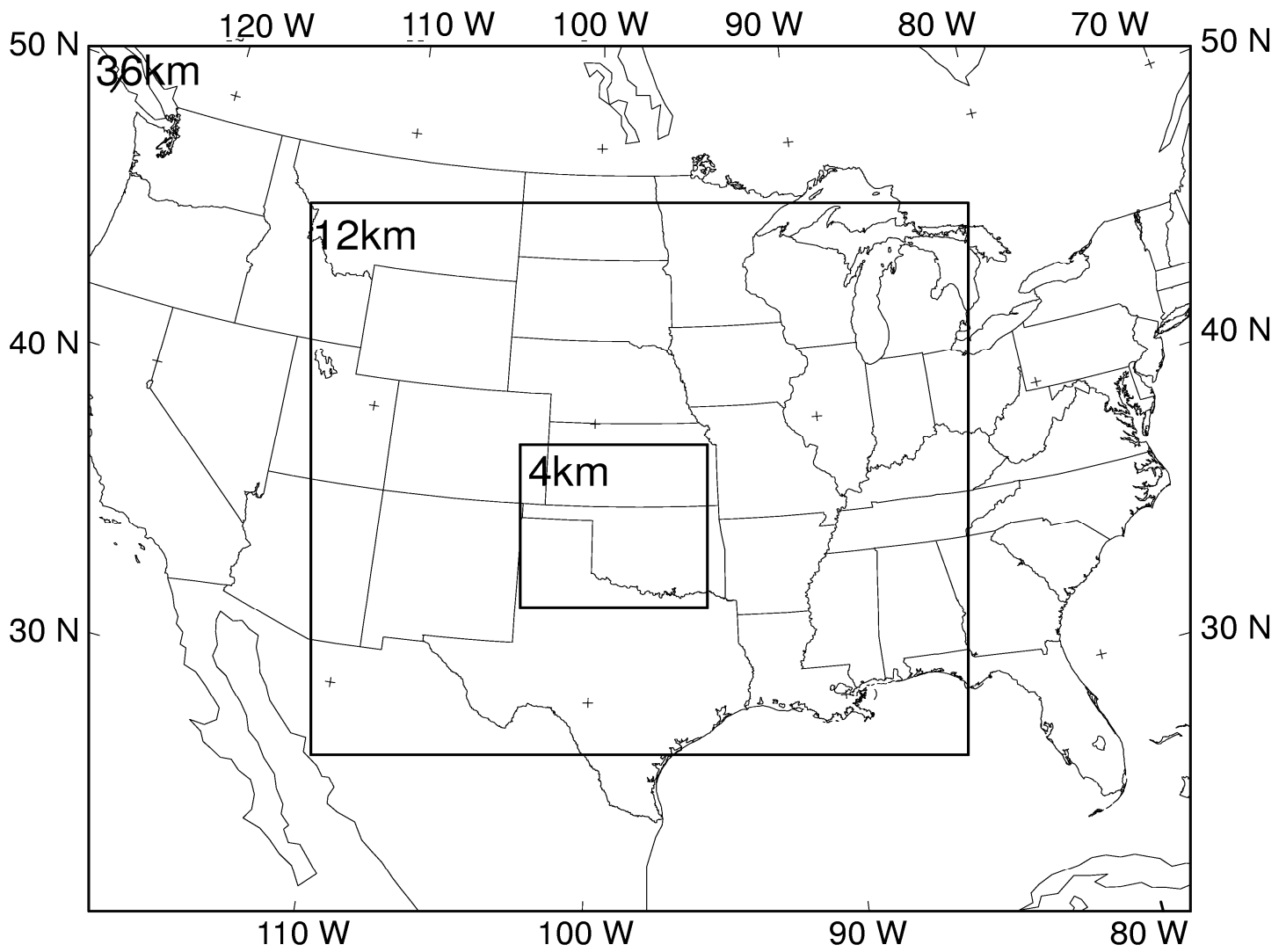
Figure 2. MM5 modeling domain used for IHOP analysis. The nested grid domains (36 km, 12 km and 4 km) are shown.
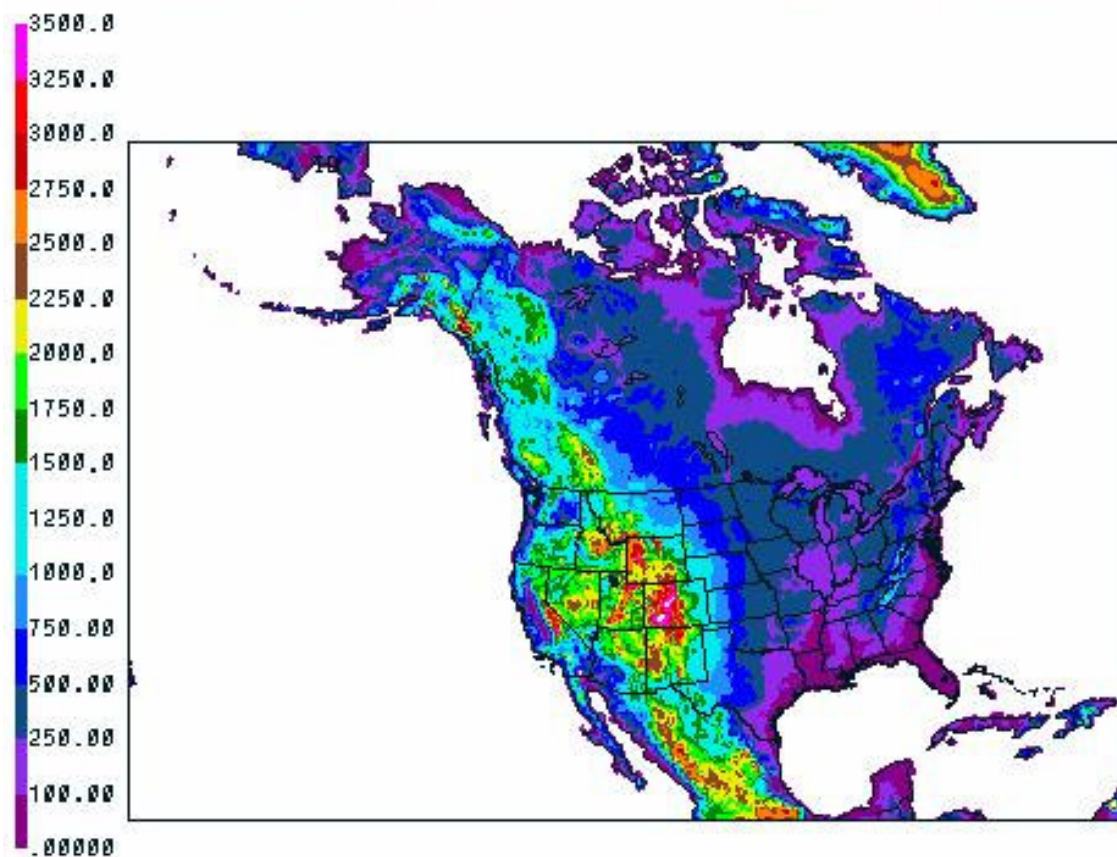
Figure 3. WRF-NMM IHOP 12 km domain with terrain elevations shown in color.
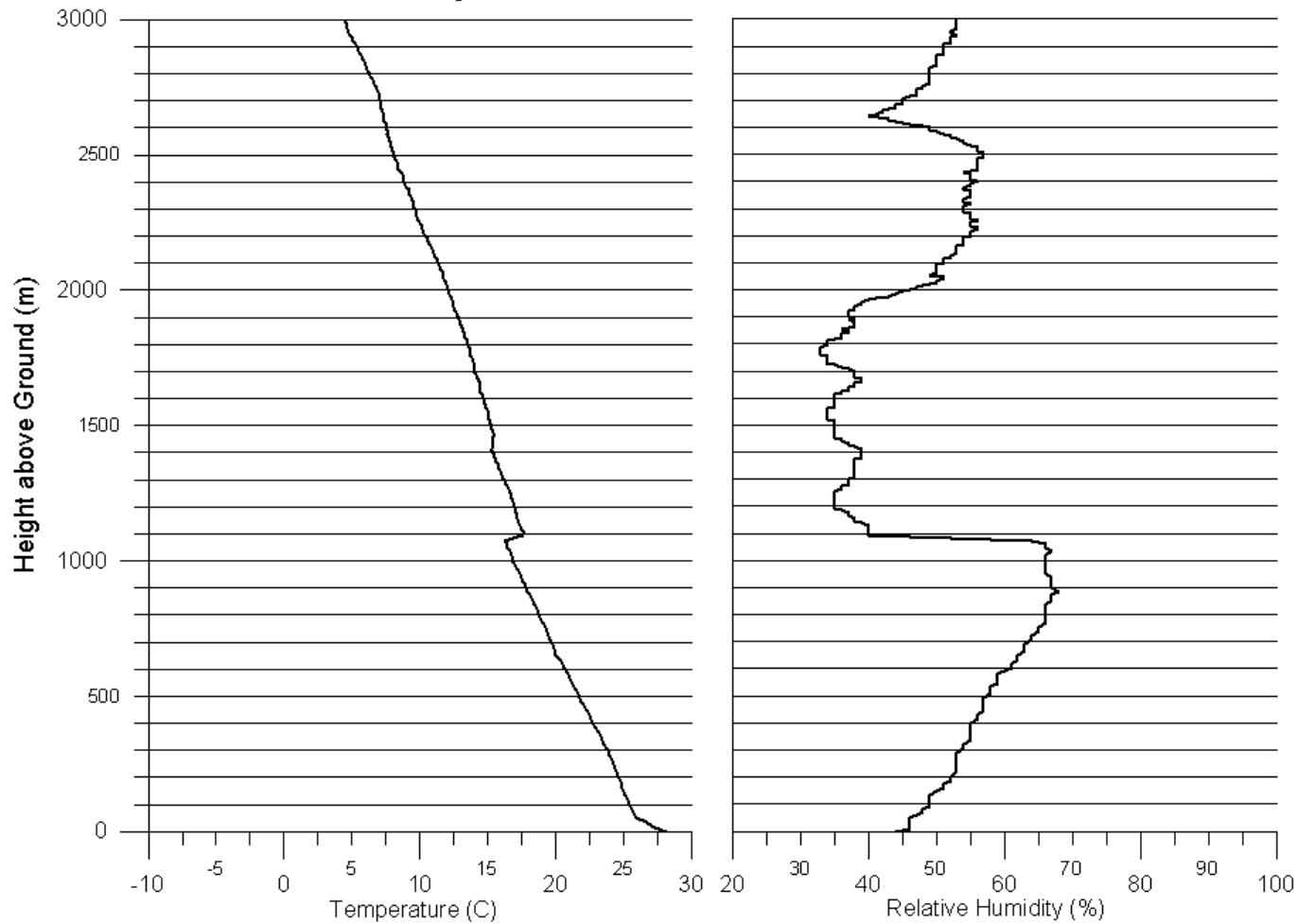
Figure 4. Example of IHOP radiosonde RH and temperature profiles where there is an obvious mixing depth, for Hillsboro, KS, at 2030 UTC on 29 May.

Balloon-Borne Sounding
Location 4 Morris, OK (Lat = 35.69, Lon = -95.86)
May 29, 2002 20:30 UTC
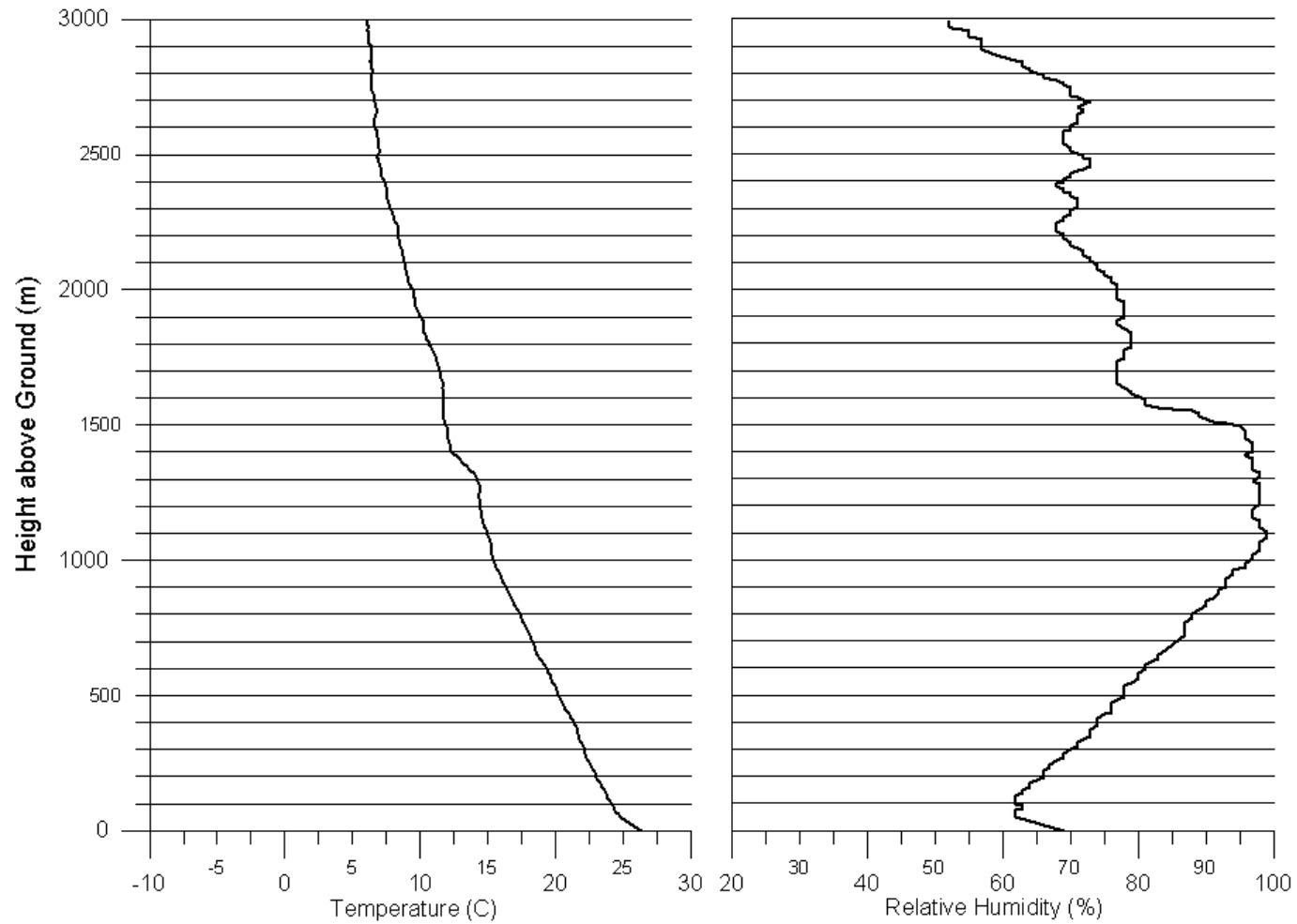
Figure 5. Example of IHOP radiosonde RH and temperature profiles where there is a vague mixing depth, for Morris, OK, at 2030 on 29 May.
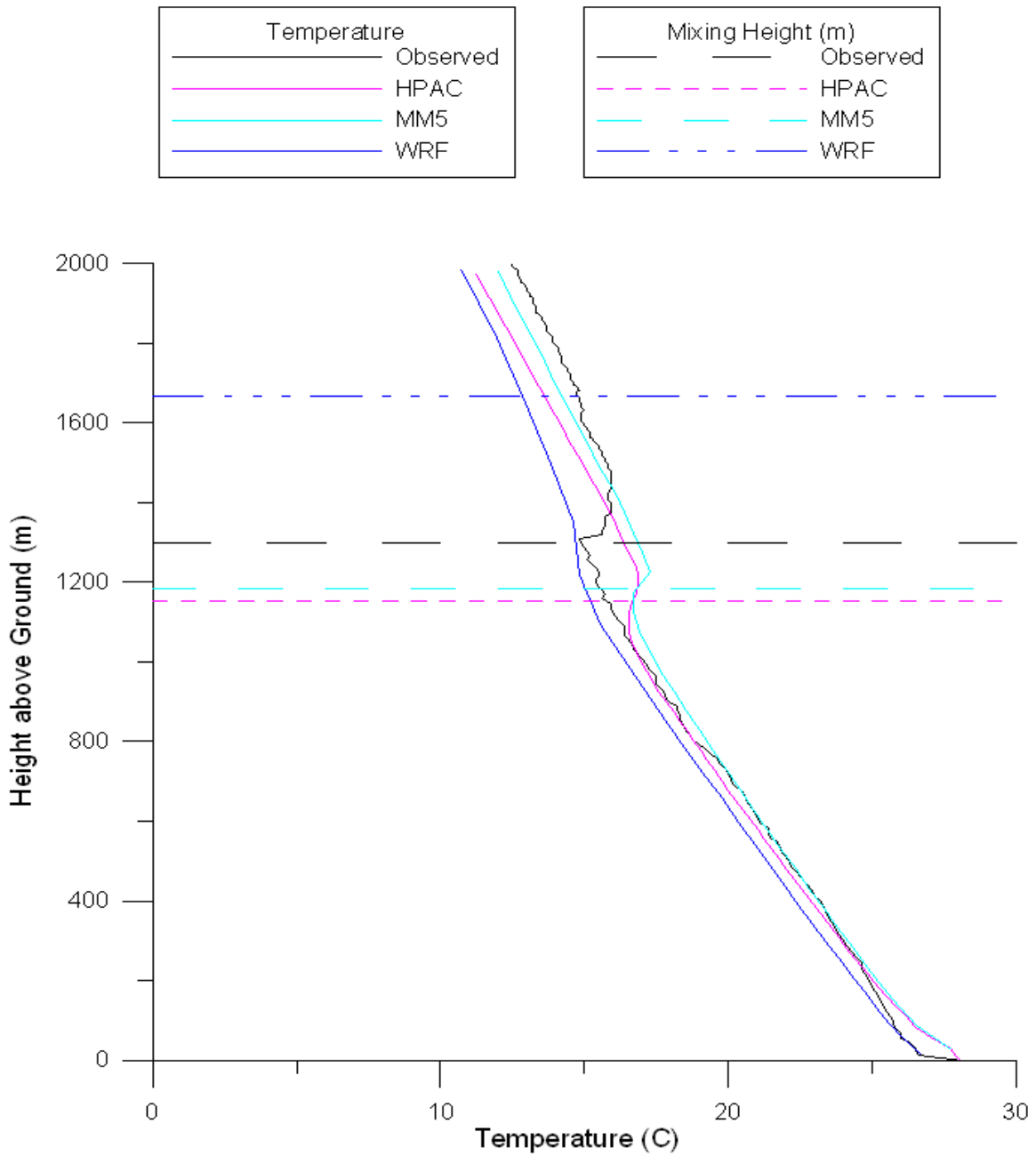
Figure 6. Example of daytime T profile comparisons, to 2000 m, for the Central Facility at 2030 UTC on 29 May.

Comparison to Balloon-Borne Sounding
Location 1 Lamont, OK (Lat = 36.61, Lon = -97.49)
May 29, 2002   8:41 UTC
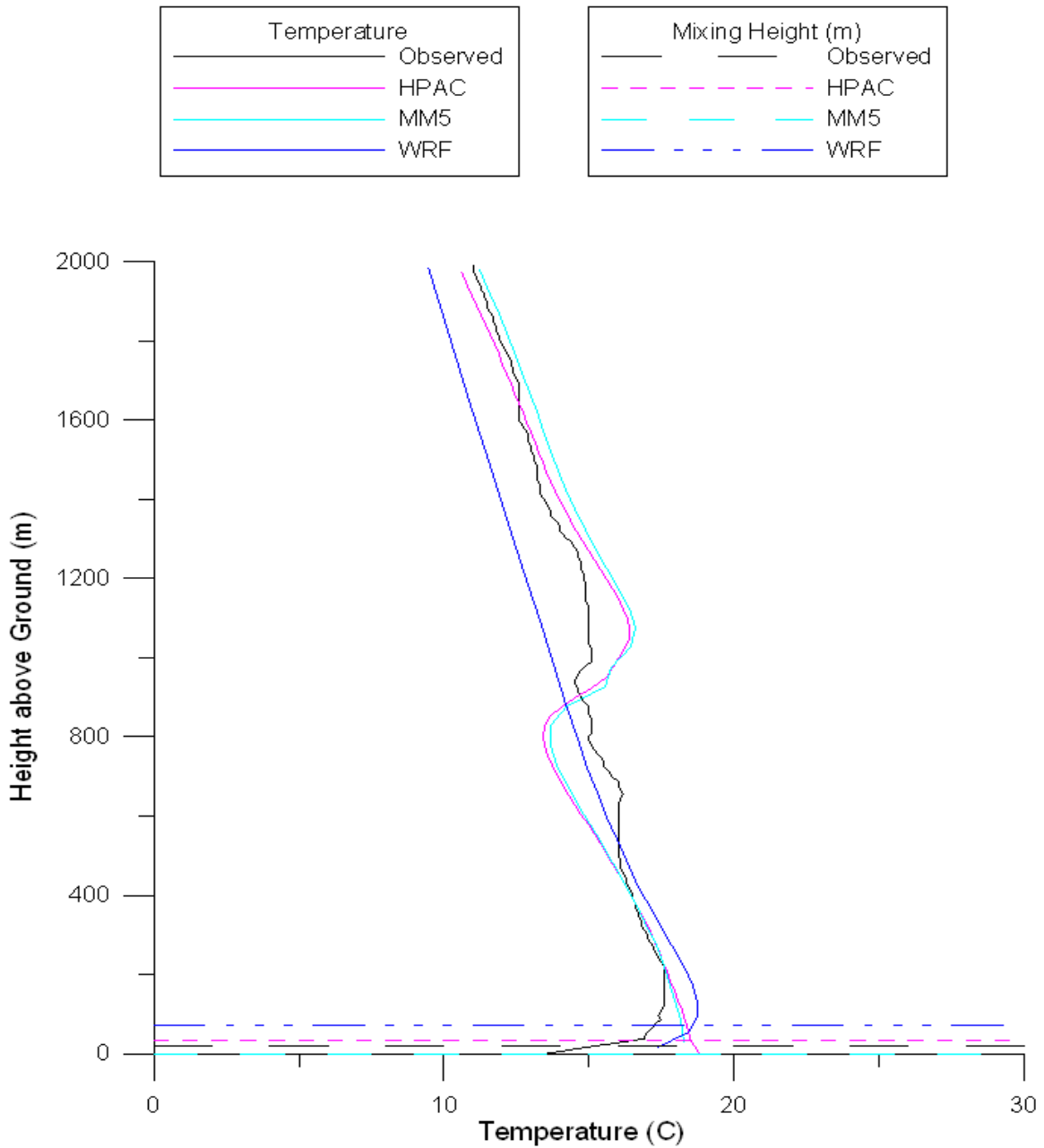
Figure 7.   Example of nighttime T profile, to 2000 m, for the Central Facility at 0841 UTC on 29 May.

Comparison to Balloon-Borne Sounding
Location 1 Lamont, OK (Lat = 36.61, Lon = -97.49)
May 29, 2002   8:41 UTC
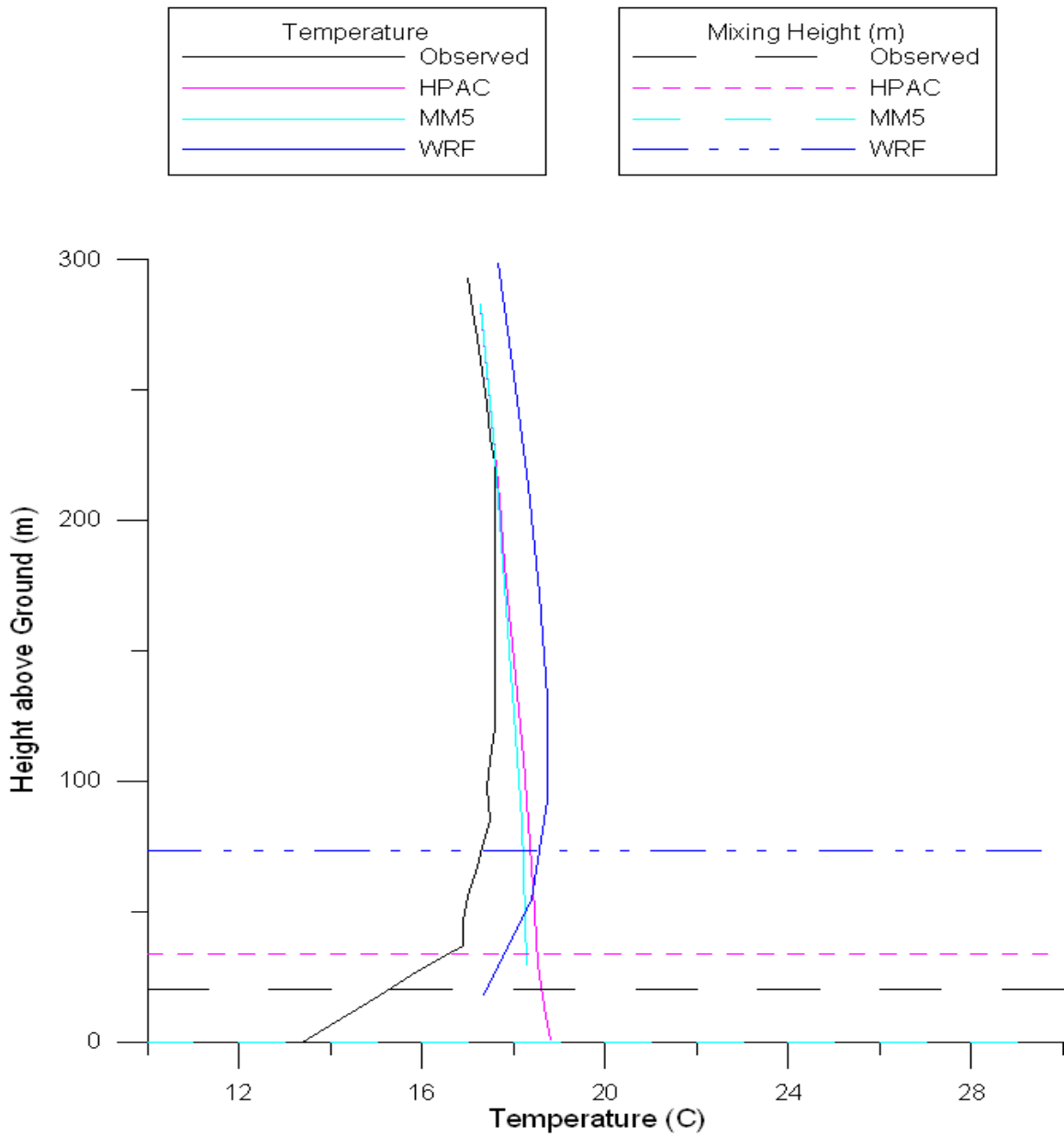
Figure 8. Example of nighttime T profile, to 300 m for the Central Facility at 0841 UTC on 29 May. This is the lower part of the profile shown in Figure 7.
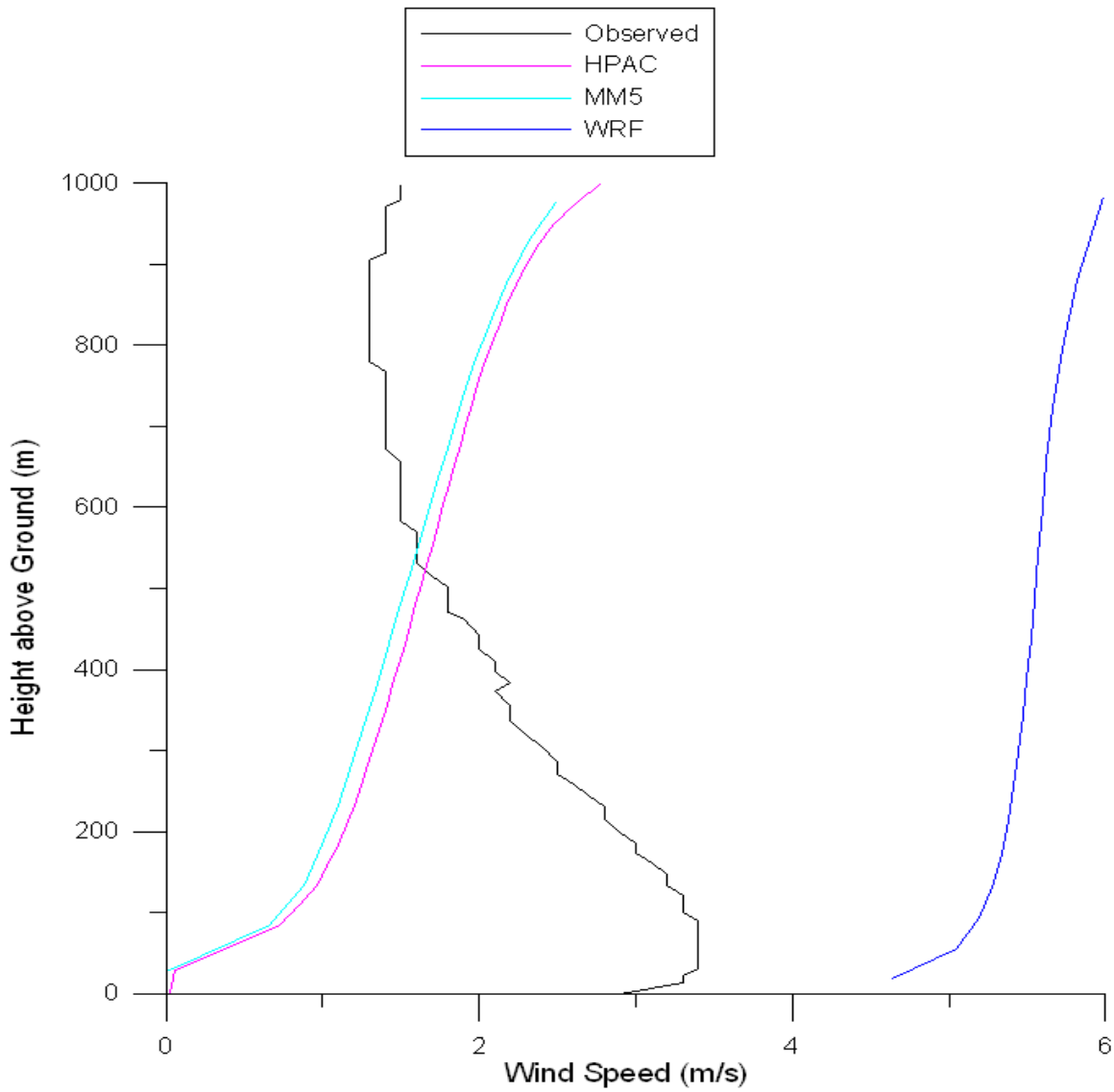
Figure 9. Example of comparison of daytime wind speeds for the Central Facility at 2030 UTC on 29 May.
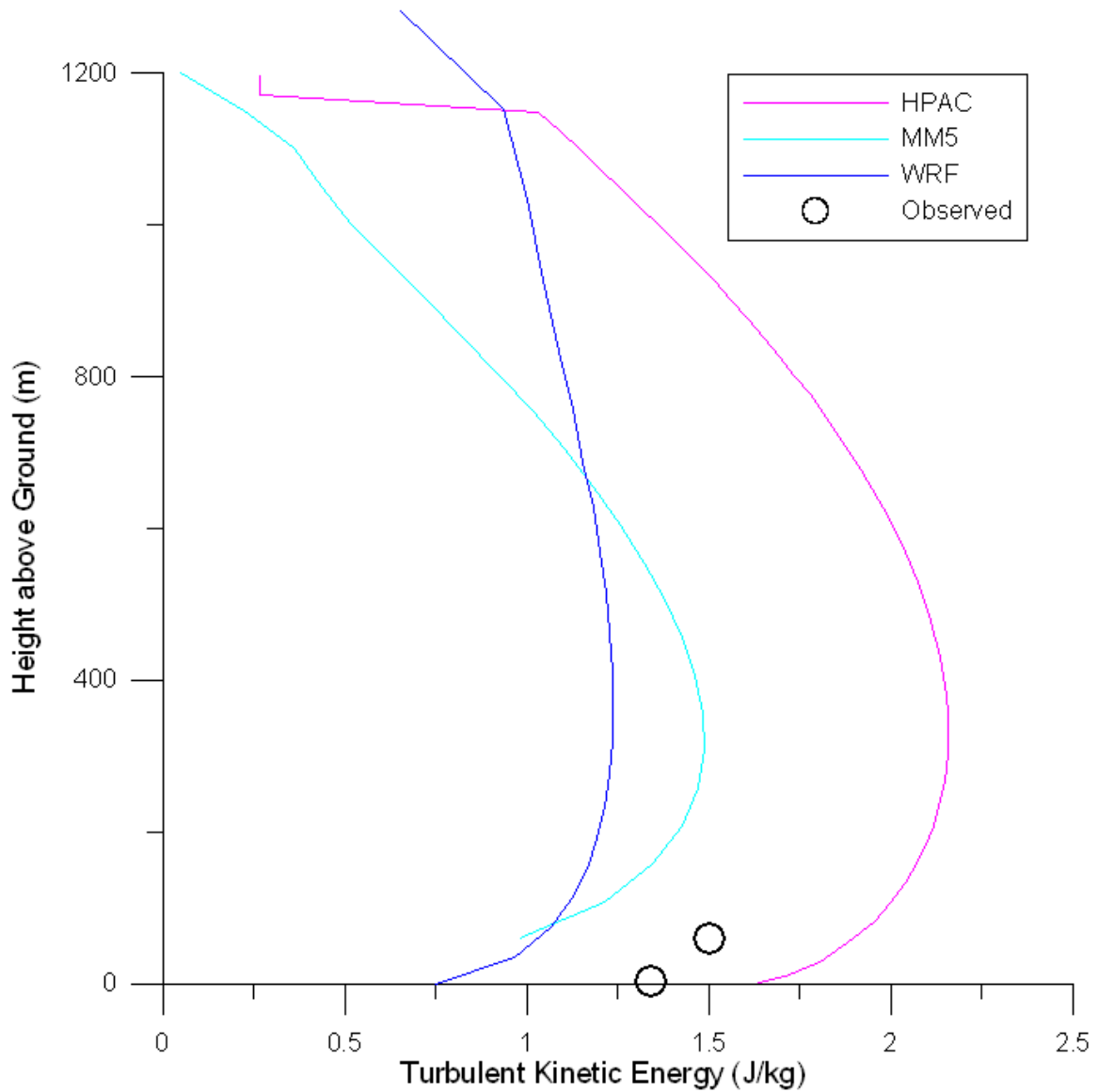
Figure 10. Example of daytime TKE comparisons, to 1200 m, for the Central Facility on 29 May.
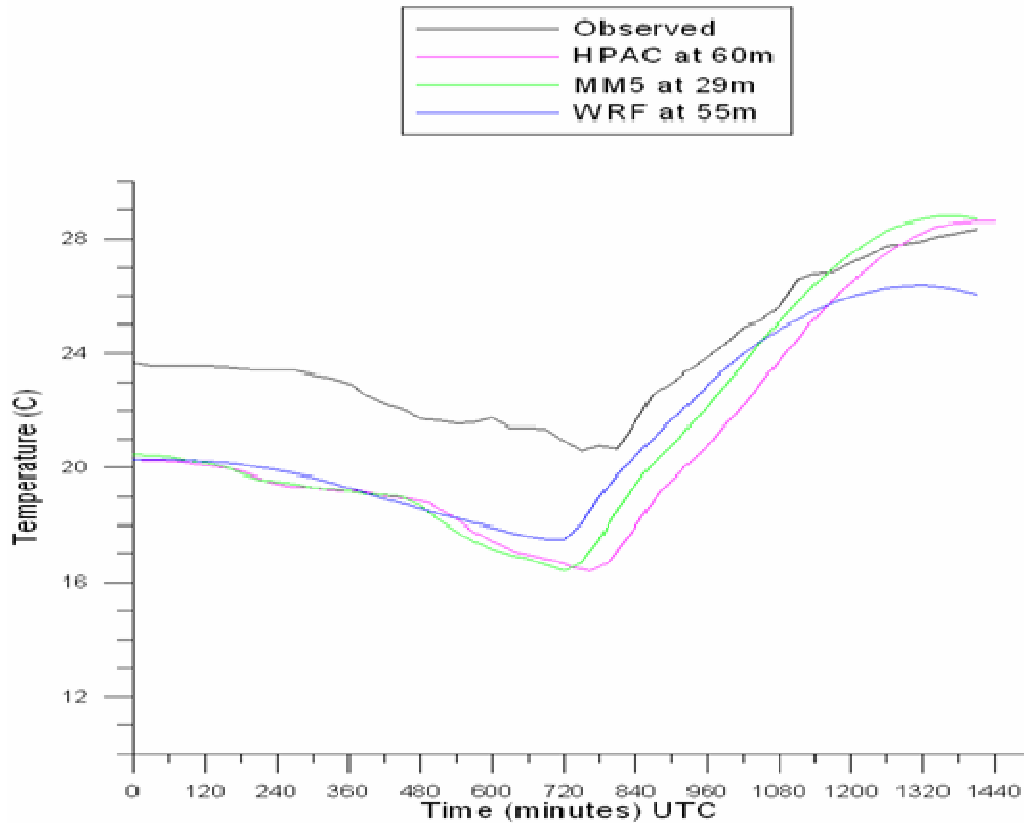
Figure 11a. Time series of observed and simulated T at Central Facility at z = 60 m on 29 May.
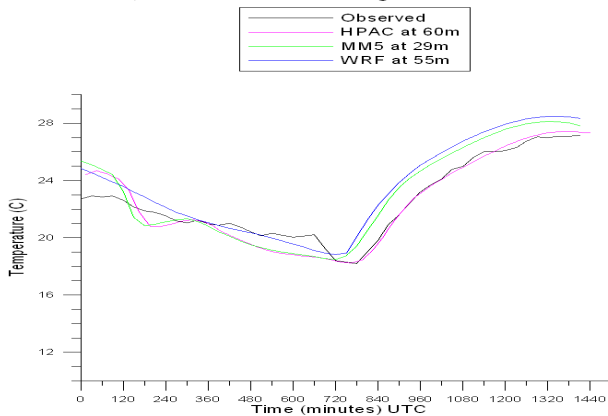
Figure 11b. Time series of observed and simulated T at Central Facility at z = 60 m on 6 June.
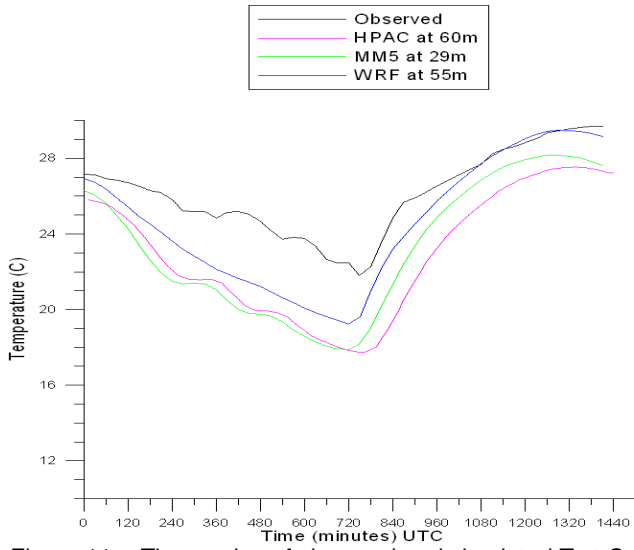
Figure 11c. Time series of observed and simulated T at Central Facility at z = 60 m on 7 June.
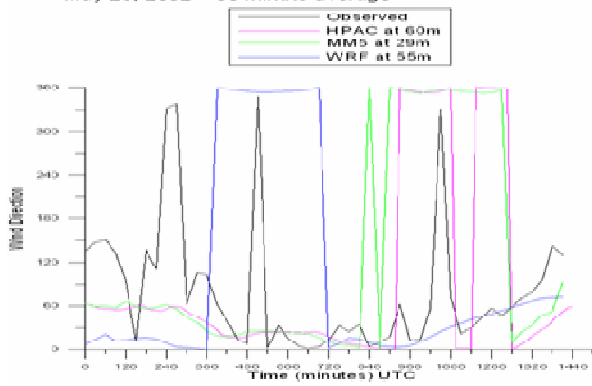
Figure 12a. Time series of observed and simulated WD at Central Facility at z = 60 m on 29 May.
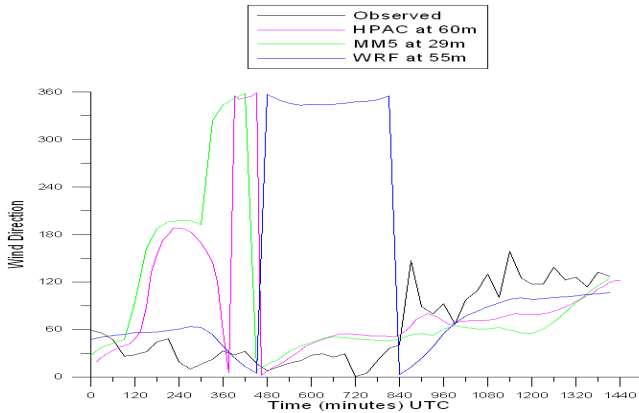
Figure 12b. Time series of observed and simulated WD at Central Facility at z = 60 m on 6 June.
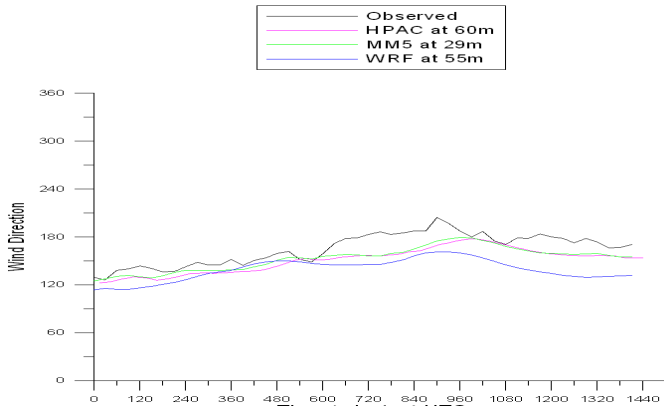
Figure 12c. Time series of observed and simulated WD at Central Facility at z = 60 m on 7 June.
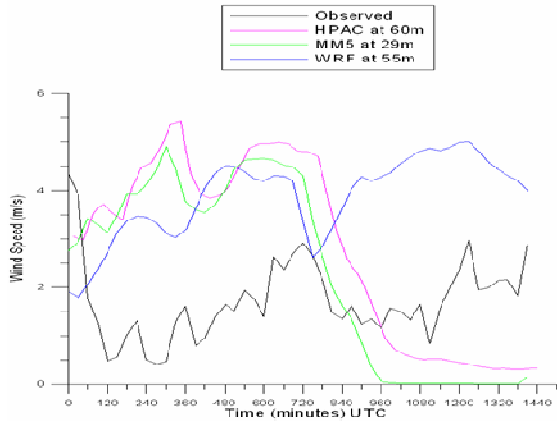
Figure 13a. Time series of observed and simulated WS at Central Facility at z = 60 m on 29 May.
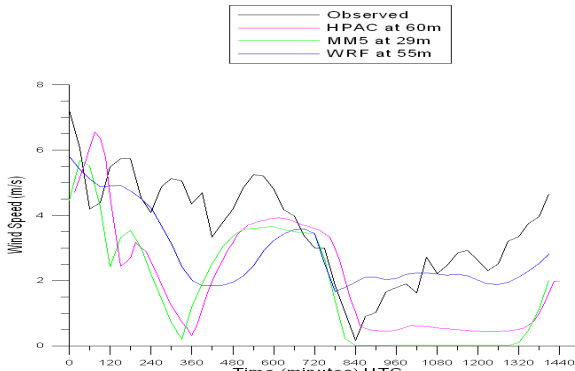
Figure 13b. Time series of observed and simulated WS at Central Facility at z = 60 m on 6 June.
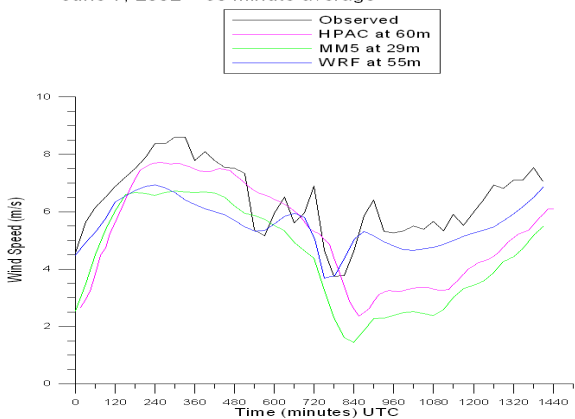
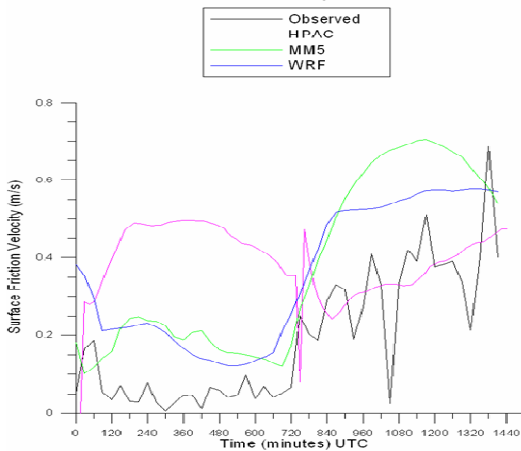*Figure 13c.* Time series of observed and simulated WS at Central Facility at z = 60 m on 7 June.
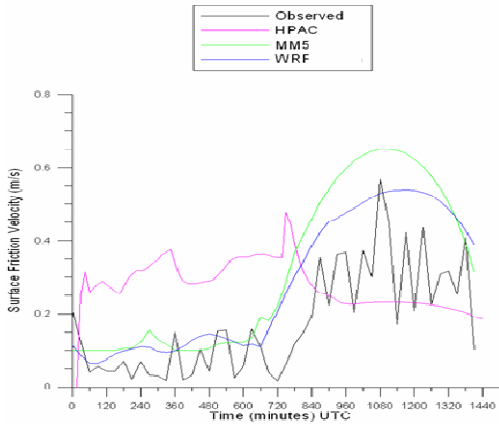
Figure 14a. Time series of observed and simulated surface friction velocity, u*, at Central Facility at z = 60 m on 29 May.
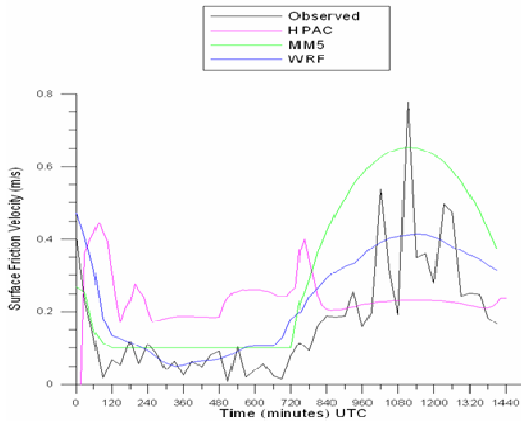
Figure 14b . Time series of observed and simulated surface friction velocity, u*, at Central Facility at z = 60 m on 6 June.

Figure 14c. Time series of observed and simulated surface friction velocity, u*, at Central Facility at z = 60 m on 7 June.
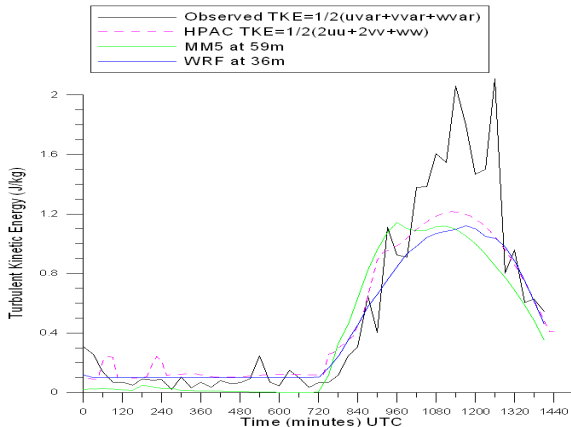
Figure 15a. Time series of observed and simulated TKE, at Central Facility at z = 60 m on 29 May.
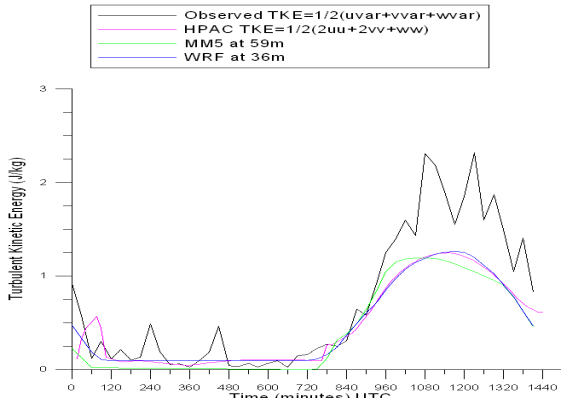
Figure 15b. Time series of observed and simulated TKE at Central Facility at z = 60 m on 6 June.
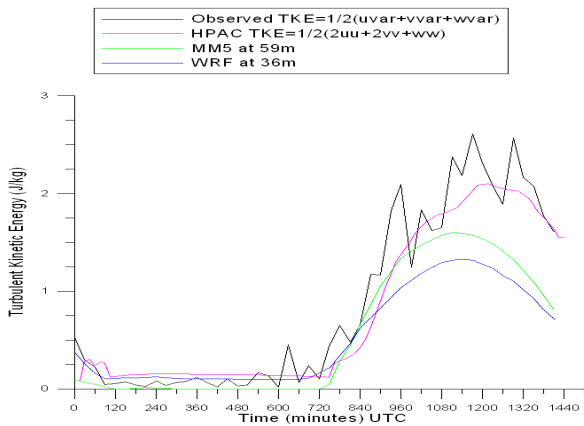
Figure 15c. Time series of observed and simulated TKE at Central Facility at z = 60 m on 7 June.

Figure 16a. Time series of observed and simulated surface buoyancy flux (SBF) at Central Facility at z = 60 m on 29 May.

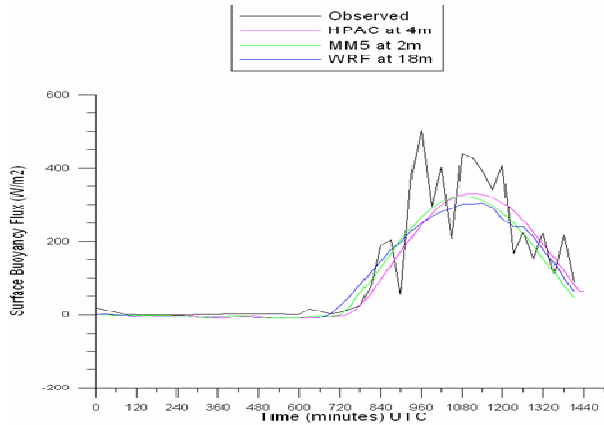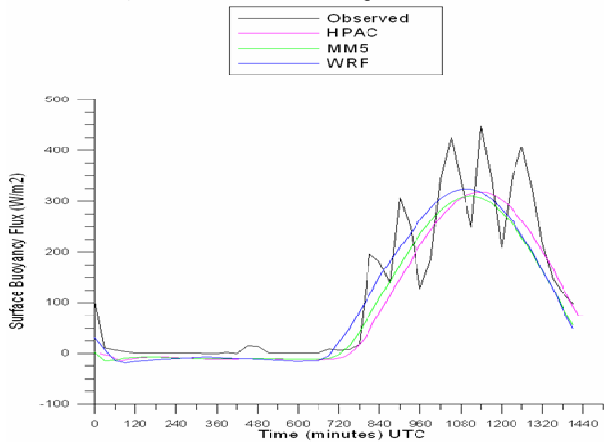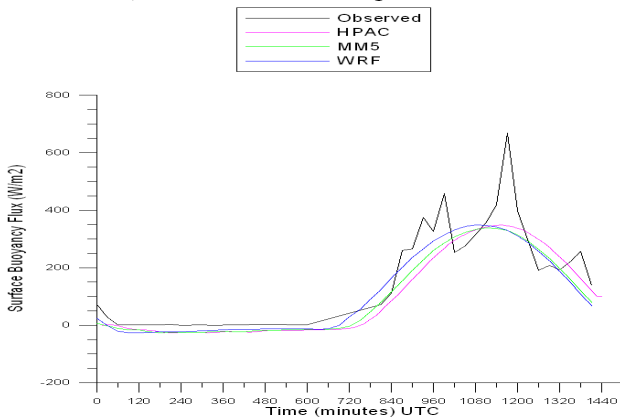*Figure 16b.* Time series of observed and simulated surface buoyancy flux (SBF) at Central Facility at z = 60 m on 6 June.

Figure 16c. Time series of observed and simulated surface buoyancy flux (SBF) at Central Facility at z = 60 m on 7 June.
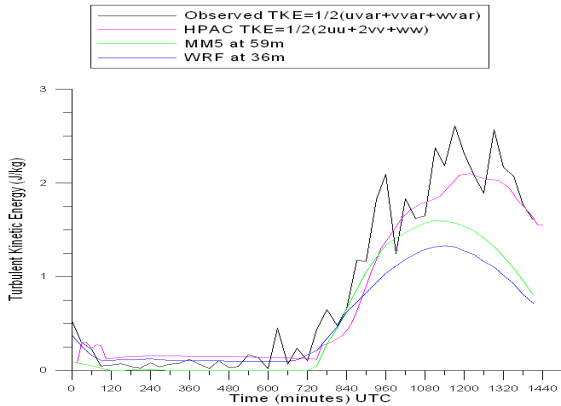
Figure 17a.   TKE time series at CF1 at z = 60 m on 7 June
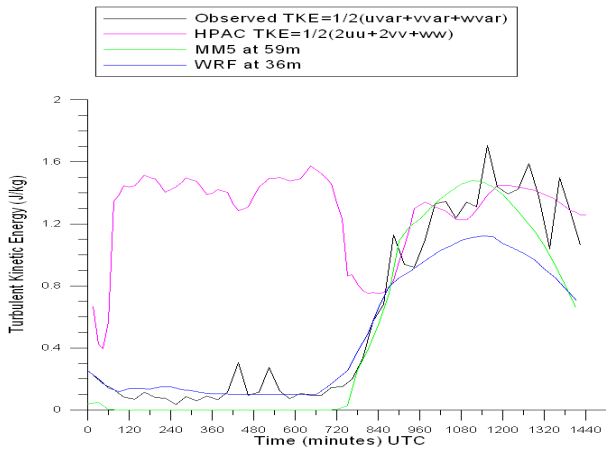
Figure 17b. TKE time series at Smileyberg at z = 2.1 m on 7 June.
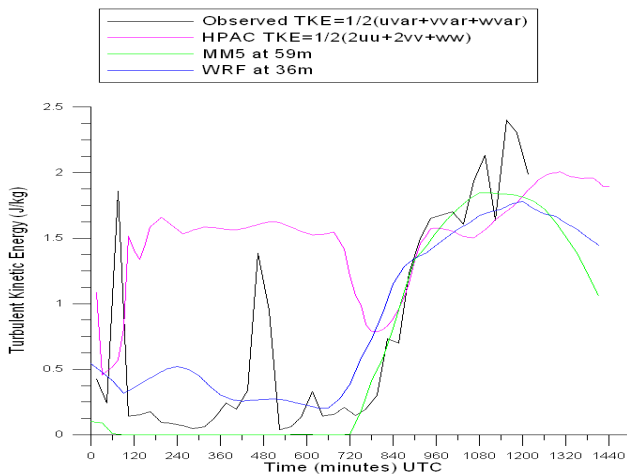
Figure 17c. TKE time series at Brainard at z = 2.1 m on 7 June.

Comparison to ISFF1 Sonic Anemometer at 2.5m
Location 8 (Lat= 36.47, Lon= -100.62)
June 7, 2002 5 minute average

Observed TKE=1/2(uvar+vvar+wvar)
HPAC TKE=1/2(2uu+2vv+ww)
MM5 at 59m
WRF at 36m
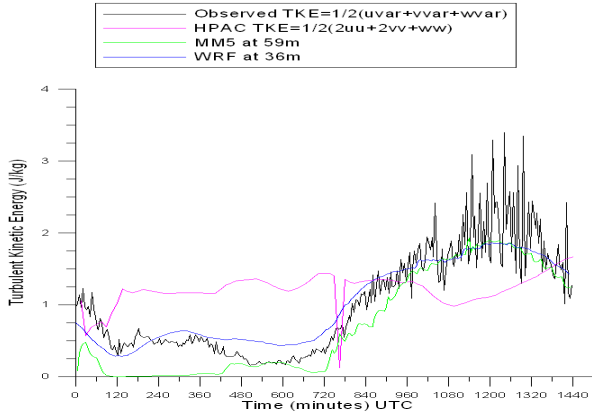
Figure 17d. TKE time series at ISSF1 z = 2.5 m on 7 June

Comparison to ISFF2 Sonic Anemometer at 3.4m
Location 9 (Lat= 36.62, Lon= -100.63)
June 7, 2002 5 minute average

Observed TKE=1/2(uvar+vvar+wvar)
HPAC TKE=1/2(2uu+2vv+ww)
MM5 at 59m
WRF at 36m
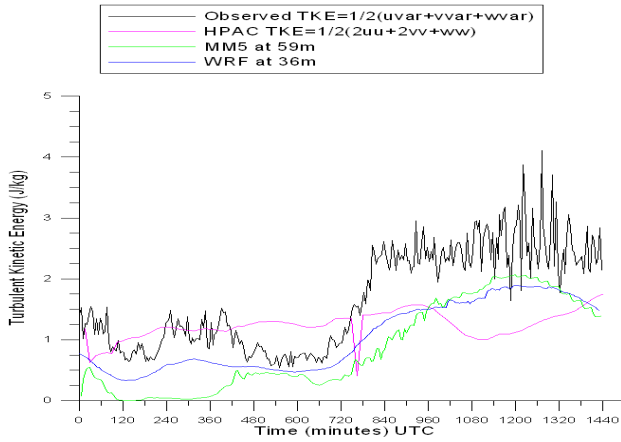
Figure 17e. TKE time series at ISSF2 z = 3.4 m on 7 June

Comparison to ISFF3 Sonic Anemometer at 2.7m
Location 10 (Lat= 36.86, Lon= -100.60)
June 7, 2002 5 minute average

Observed TKE=1/2(uvar+vvar+wvar)
HPAC TKE=1/2(2uu+2vv+ww)
MM5 at 59m
WRF at 36m
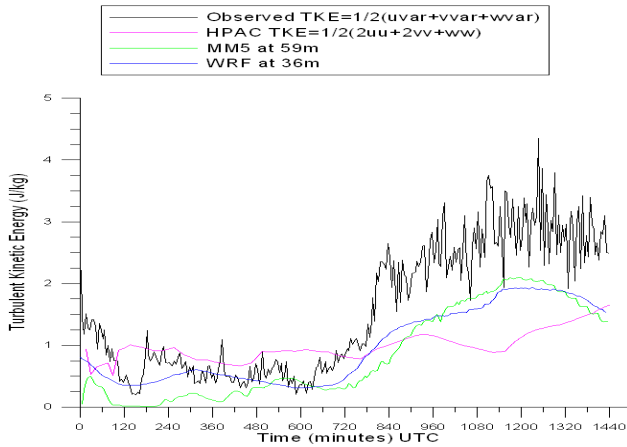
Figure 17f. TKE time series at ISSF3 z = 2.7 m on 7 June
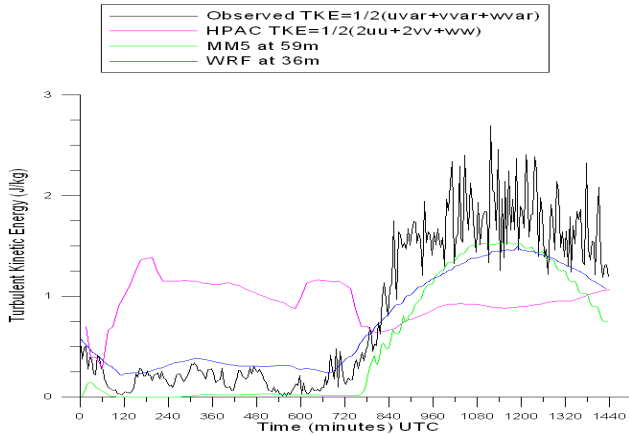
Figure 17g. TKE time series at ISSF4 z = 2.6 m on 7 June
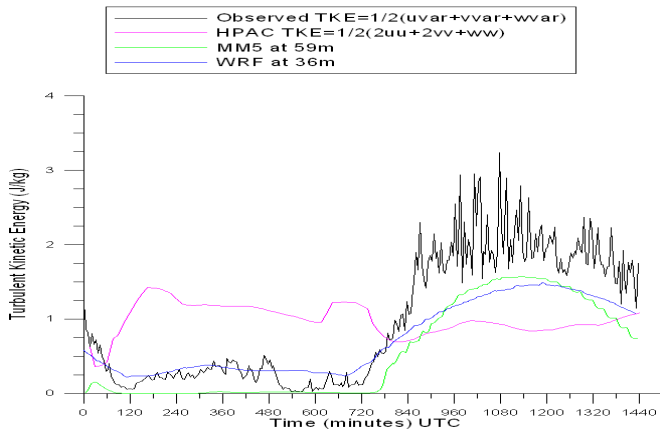
Figure 17h. TKE time series at ISSF5 z = 5 m on 7 June
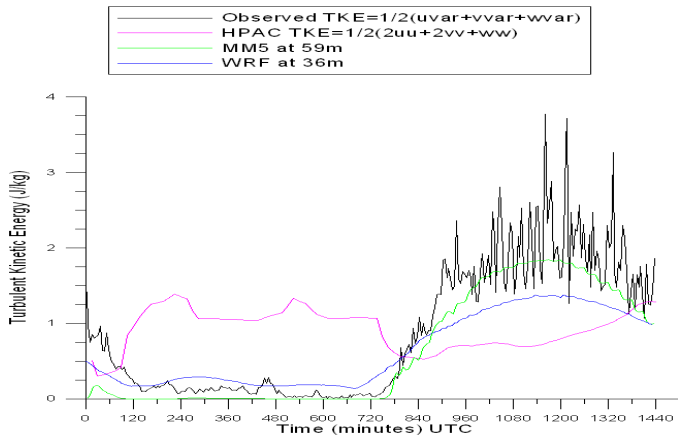
Figure 17i. TKE time series at ISSF6 z = 4.9 m on 7 June
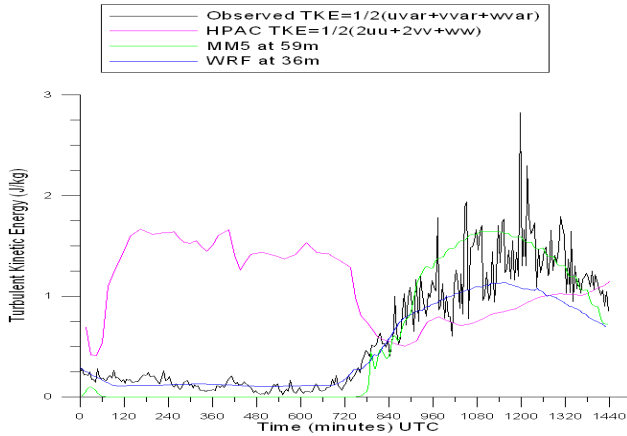
Figure 17j. TKE time series at ISSF7 z = 2.7 m on 7 June
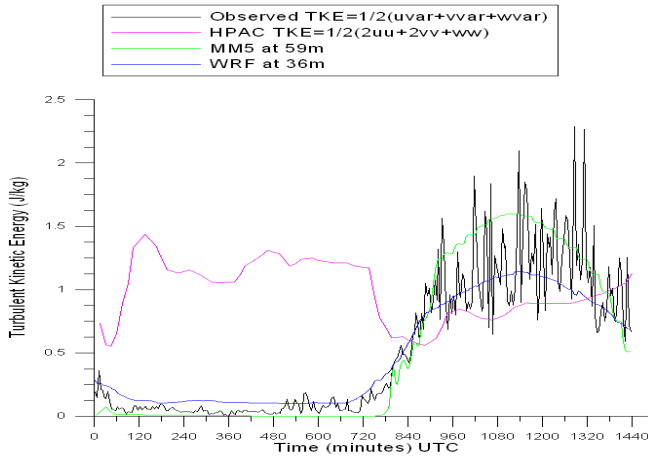
Figure 17k. TKE time series at ISSF8 z = 4.6 m on 7 June
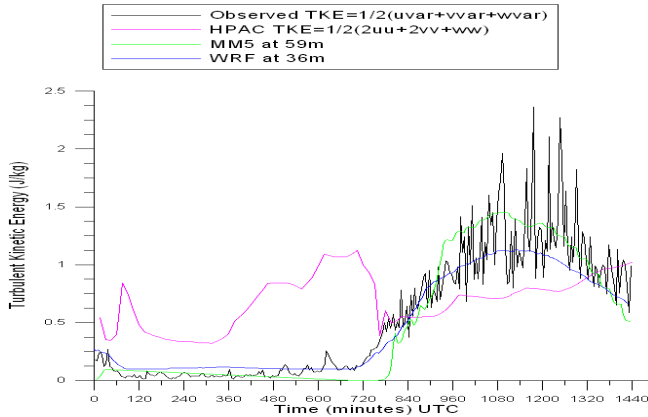
Figure 17l. TKE time series at ISSF9 z = 4.7 m on 7 June.

Appendix A - Description of MM5 and WRF-NMM Outputs

A-1 MM5 Model Outputs

The MM5 model outputs were provided in a time series format. Coding was added to the MM5 model to produce all parameters in the standard MM5 output file at every time step at the sixteen IHOP locations. TSREAD reads in binary time series output from MM5 or WRF-NMM, extracts desired variables (including any averaging specified by the user), and outputs a file from which TSPLOT can create figures. TSPLOT reads in binary time series output from TSREAD and uses NCAR Graphics to create time series and profile plots as specified by the user. In addition to the plots, TSPLOT also outputs a text file of the parameters specified by the user. This software was written in Fortran 90 and designed to run in a UNIX environment.

TSREAD was run twice for each file, once to create 5-minute averages and a second time to create 30-minute averages. TSPLOT was run on the TSREAD processed files to extract profiles from the 5-minute averages, and time series from both the 5-minute and 30-minute averages. The text file that TSPLOT creates was transferred to a PC and the Windows based GRAPHER7 software was used to create the plots of modeled and observed parameters.

Table A-1 lists the MM5 parameters output in the time series files (TSREAD diagnostic output). A description of the information column can be found at the end of the table.

Table A-1: MM5 Parameters Output to the Time Series Files for the IHOP Site Locations

| Variable	Description	Units	Information*
PSTARCRS	(REFERENCE) SURFACE PRESSURE MINUS PTOP	Pa	2 C X R
GROUND T	GROUND TEMPERATURE	K	2 C X R
RAIN CON	ACCUMULATED CONVECTIVE PRECIPITATION	cm	2 C X R
RAIN NON	ACCUMULATED NONCONVECTIVE PRECIPITATION	cm	2 C X R
TERRAIN	TERRAIN ELEVATION	m	2 C X R
MAPFACCR	MAP SCALE FACTOR	N/A	2 C X R
CORIOLIS	CORIOLIS PARAMETER	1/s	2 C X R
RES TEMP	INFINITE RESERVOIR SLAB TEMPERATURE	K	2 C X R
LATITCRS	LATITUDE (SOUTH NEGATIVE)	DEGREES	2 C X R
LONGICRS	LONGITUDE (WEST NEGATIVE)	DEGREES	2 C X R
LAND USE	LANDUSE CATEGORY	category	2 C X R
TSEASFC	SEA SURFACE TEMPERATURE	K	2 C X R
PBL HGT	PBL HEIGHT	m	2 C X R
REGIME	PBL REGIME	N/A	2 C X R
SHFLUX	SENSIBLE HEAT FLUX	W/m^2	2 C X R
LHFLUX	LATENT HEAT FLUX	W/m^2	2 C X R
UST	FRICTIONAL VELOCITY	m/s	2 C X R
SWDOWN	SURFACE DOWNWARD SHORTWAVE RADIATION	W/m^2	2 C X R
LWDOWN	SURFACE DOWNWARD LONGWAVE RADIATION	W/m^2	2 C X R
SWOUT	TOP OUTGOING SHORTWAVE RADIATION	W/m^2	2 C X R
LWOUT	TOP OUTGOING LONGWAVE RADIATION	W/m^2	2 C X R
SBF	SURFACE BUOYANCY FLUX	W/m^2	2 C X R
MONIN	MONIN LENGTH	m	2 C X R
WSTAR	CONVECTIVE VELOCITY	m/s	2 C X R
ZNT	ROUGHNESS LENGTH	m	2 C X R
CANOPYM	CANOPY MOISTURE CONTENT	m	2 C X R
WEASD	WATER EQUIVALENT SNOW DEPTH	mm	2 C X R
SNOWH	PHYSICAL SNOW DEPTH	m	2 C X R
SNOWCOVR	FRACTIONAL SNOW COVER	fraction	2 C X R
ALB	ALBEDO	fraction	2 C X R
GRNFLX	GROUND HEAT FLUX	W/m^2	2 C X R
VEGFRC	VEGETATION COVERAGE	percent	2 C X R
SEAICE	SEA ICE FLAG	N/A	2 C X R
SFCRNOFF	SURFACE RUNOFF	mm	2 C X R
UGDRNOFF	UNDERGROUND RUNOFF	mm	2 C X R
SOILINDX	DOMINANT TYPE SOIL CATEGORY	category	2 C X R
SOIL T 1	SOIL TEMPERATURE IN LAYER 1	K	2 C X R
SOIL T 2	SOIL TEMPERATURE IN LAYER 2	K	2 C X R

SOIL T 3	SOIL TEMPERATURE IN LAYER 3	K	2 C X R
SOIL T 4	SOIL TEMPERATURE IN LAYER 4	K	2 C X R
SOIL M 1	TOTAL SOIL MOIS IN LYR 1	m^3/m^3	2 C X R
SOIL M 2	TOTAL SOIL MOIS IN LYR 2	m^3/m^3	2 C X R
SOIL M 3	TOTAL SOIL MOIS IN LYR 3	m^3/m^3	2 C X R
SOIL M 4	TOTAL SOIL MOIS IN LYR 4	m^3/m^3	2 C X R
SOIL W 1	SOIL LQD WATER IN LYR 1	m^3/m^3	2 C X R
SOIL W 2	SOIL LQD WATER IN LYR 2	m^3/m^3	2 C X R
SOIL W 3	SOIL LQD WATER IN LYR 3	m^3/m^3	2 C X R
SOIL W 4	SOIL LQD WATER IN LYR 4	m^3/m^3	2 C X R
T2	2-METER TEMPERATURE	K	2 C X R
Q2	2-METER WATER VAPOR MIXING RATIO	kg/kg	2 C X R
RAINRTC	CONVECTIVE RAIN RATE	cm/hr	2 C X D
RAINRTNC	NONCONVECTIVE RAIN RATE	cm/hr	2 C X D
U	U COMPONENT OF HORIZONTAL WIND	m/s	3 C H R
V	V COMPONENT OF HORIZONTAL WIND	m/s	3 C H R
T	TEMPERATURE	K	3 C H R
Q	MIXING RATIO	kg/kg	3 C H R
CLW	CLOUD WATER MIXING RATIO	kg/kg	3 C H R
RNW	RAIN WATER MIXING RATIO	kg/kg	3 C H R
TKE	TURBULENT KINETIC ENERGY	J/kg	3 C F R
RAD TEND	ATMOSPHERIC RADIATION TENDENCY	K/day	3 C H R
W	VERTICAL WIND COMPONENT	m/s	3 C F R
PP	PRESSURE PERTURBATION	Pa	3 C H R
KTH3D	THERMAL EDDY DIFFUSIVITY	m^2/s	3 C F R
KZM3D	MOMENTUM EDDY DIFFUSIVITY	m^2/s	3 C F R
LH3D	THERMAL MIXING LENGTH	m	3 C F R
LM3D	MOMENTUM MIXING LENGTH	m	3 C F R
SHF3D	SENSIBLE HEAT FLUX	W/m^2	3 C F R
LHF3D	LATENT HEAT FLUX	W/m^2	3 C F R
PMB	PRESSURE, HALF LAYER	mb	3 C H R
PMBF	PRESSURE, FULL LAYER	mb	3 C F R
UFLUX	U MOMENTUM FLUX	m^2/s^2	3 C F R
VFLUX	V MOMENTUM FLUX	m^2/s^2	3 C F R
BOU3D	BOUYANCY TKE TEND TERM	J/kg s-1	3 C F R
SHEAR3D	SHEAR TKE TEND TERM	J/kg s-1	3 C F R
DISSIP3D	DISSIPATION TKE TEND TERM	J/kg s-1	3 C F R
TURB3D	TURB TRANSPORT TKE TEND TERM	J/kg s-1	3 C F R
THETA	POTENTIAL TEMPERATURE	K	3 C H R
WNDSPEED	WIND SPEED	m/s	3 C H D
WIND DIR	WIND DIRECTION	DEGREES	3 C H D

* Variable Information Description
        Column 1 = Dimension of original variable
        Column 2 = Cross point (C) or dot point (D)
        Column 3 = Half level (H), full level (F), or not applicable (X)
        Column 4 = Read from input file (R) or diagnosed in TSREAD (D)

A.2 WRF-NMM Model Outputs

    The WRF-NMM model outputs were provided by NCEP in a binary time series format. They were in a similar format to the MM5 outputs so that the TSREAD and TSPLOT software could be used to time average and plot the WRF-NMM outputs. One difference in format was that the WRF outputs were provided in 48 files, one for each of the 16 IHOP sites for each of the three days. Each of the model runs was initialized 12 hours before the day of interest. The model outputs were made available on the NCEP ftp site for downloading. The WRF-NMM output files were processed similarly to the MM5 outputs using TSREAD and TSPLOT. The initial processing was done in a UNIX environment and then the extracted variables were plotted on a PC in a Windows environment.

    Table A-2 lists the WRF-NMM parameters output in the time series files (TSREAD diagnostic output). A description of the information column can be found at the end of the table.

Table A-2. WRF-NMM Parameters Output to the Time Series Files for the IHOP Site Locations

Variable	Description	Units	Information*
TERRAIN	TERRAIN HEIGHT	m	2 C X R
ZNT	ROUGHNESS LENGTH	m	2 C X R
PBL HGT	PBL HEIGHT	m	2 C X R
SBF	SURFACE BUOYANCY FLUX	W/m^2	2 C X R
UST	USTAR	m/s	2 C X R
MONIN	MONIN OBUKHOV LENGTH	m	2 C X R
WSTAR	CONVECTIVE VELOCITY	m/s	2 C X R
LATITCRS	ACTUAL LATITUDE		2 C X R
LONGICRS	ACTUAL LONGITUDE		2 C X R
SHFLUX	SURFACE SENSIBLE HEAT FLUX	W/m^2	2 C X R
LHFLUX	SURFACE LATENT HEAT FLUX	W/m^2	2 C X R
RAINRTC	CONVECTIVE RAIN RATE		2 C X D
RAINRTNC	NONCONVECTIVE RAIN RATE		2 C X D
PMB	PRESSURE, HALF LAYER	mb	3 C H R
PMBF	PRESSURE, FULL LAYER	mb	3 C F R
U	U COMPONENT OF HORIZONTAL WIND	m/s	3 C H R
V	V COMPONENT OF HORIZONTAL WIND	m/s	3 C H R
W	VERTICAL WIND COMPONENT	m/s	3 C H R
T	TEMPERATURE	K	3 C H R
Q	SPECIFIC HUMIDITY	kg/kg	3 C H R
CLW			3 C H R
TKE	TURBULENT KINETIC ENERGY	J/kg	3 C F R
LH3D	THERMAL MIXING LENGTH	m	3 C H R
LM3D	MOMENTUM MIXING LENGTH	m	3 C H R
WNDSPEED	WIND SPEED	m/s	3 C H D
WIND DIR	WIND DIRECTION	DEGREES	3 C H D

* Variable Information Description

        Column 1 = Dimension of original variable
        Column 2 = Cross point (C) or dot point (D)
        Column 3 = Half level (H), full level (F), or not applicable (X)
        Column 4 = Read from input file (R) or diagnosed in tsread (D)

Note: Blanks in the above table reflect blanks in the TSREAD output when processing WRF model output.

Appendix B - HPAC/SCIPUFF Parameterized Meteorology

    HPAC/SCIPUFF directly accepts inputs of wind speed, wind direction, and temperature profiles, mixing depths (PBL heights), and surface buoyancy flux from the meteorological models MM5 or WRF-NMM. To streamline the transfer to HPAC/SCIPUFF, the meteorological model outputs are first converted to a so-called MEDOC file. HPAC/SCIPUFF then uses idealized boundary layer representations to generate vertical profiles of the three components of turbulence: $\sigma_u^2 = \langle u'u' \rangle$, $\sigma_v^2 = \langle v'v' \rangle$, and $\sigma_w^2 = \langle w'w' \rangle$, as well as the turbulent integral length scales for the three components. It would be possible to use the HPAC/SCIPUFF internal formulas to directly calculate these variables. However, it is easier to simply use the model capability to output "meteorological profiles" at the specific IHOP sites.

    To generate the output meteorological profiles, HPAC version 4.04.011 was used to simulate a fictitious release using the MEDOC files created from the MM5 files. Both 5-minute and 30-minute time averaged MM5 MEDOC files were used. A "Met sampler" file was used to output meteorological variables from HPAC at the desired heights and times. Table B-1 shows the variables that are output by HPAC with their definitions and units.

Table B-1. Meteorological Variables Output by HPAC with "Met" Sampler File

Variable Name	Variable Definition	Variable Unit
U*	*x*-component velocity	Meters per second
V*	*y*-component velocity	Meters per second
W*	*z*-component velocity	Meters per second
T*	Absolute Temperature	Degrees Kelvin
ZI*	Boundary Layer Depth	Meters
HFLX*	Surface Heat Flux	K-m/s
L	Monin-Obukhov Length	Meters
UU	Shear-driven turbulence	Meter squared per second squared
VV	Buoyancy-driven turbulence	Meter squared per second squared
WW	Vertical velocity correlation	Meter squared per second squared

* These parameters are input to HPAC through the MM5 MEDOC file.

    A post-processor was developed to read the sampler output files generated by HPAC and to create individual files which were easier to plot.

    The temperature in the HPAC output is supposed to be the same as that in the meteorological model outputs that are given to HPAC. However, there was a slight error in the conversion factor for potential temperature. An adjustment factor was derived to correct for the fact that the HPAC code uses the wrong reference pressure in its calculation. The output temperature was multiplied by the following dimensionless conversion factor:

$$T_{conv} = (1013.25/1000)^{2/7}$$

    The surface buoyancy flux was calculated from the surface heat flux that HPAC outputs using the following equation:

SBF (W/m^2) = HFLX ρ c_p

where
    ρ is the density of air (29/0.0821/T(K) kg/m^3),
    c_p is the heat capacity of air (1004 J/kg/K)

    In addition, the temperature in K was converted to C, the mixing depth (PBL height) was adjusted to be above the ground, wind speed and direction were calculated from the horizontal velocity components, and the turbulent kinetic energy (TKE) was calculated from the velocity correlations in HPAC as follows:

HPAC TKE = ½*(2*UU + 2*VV + WW)

The factor of two before the UU and VV occur due to the fact that UU represents the shear-driven component and VV represents the buoyancy driven component and the two must be added together to get the total horizontal velocity variance, i.e.:

$\langle v'v' \rangle$ = UU + VV

        and;

$\langle u'u' \rangle$ = $\langle v'v' \rangle$

    The y-component of the horizontal velocity variance $\langle v'v' \rangle$ is calculated as the total of the shear-driven and buoyancy driven contributions. And, the x-component $\langle u'u' \rangle$ is assumed to be equal to $\langle v'v' \rangle$.

Therefore, the post-processor also added these two components together to be compared to the observations.

Since the observations represent a finite time average, while the HPAC/SCIPUFF output variables represent an ensemble average, the HPAC/SCIPUFF velocity variances were adjusted when comparing to the observed calculations for the time series plots. The profile plots do not have an adjustment for the time average, since these plots compare the meteorological model outputs with HPAC/SCIPUFF, and all are ensemble variances. The original and adjusted HPAC TKE and variances are both shown on the time series plots; the adjusted is called "HPAC for Obs".

The variance adjustment to account for the finite observational time average uses the methodology from HPAC/SCIPUFF to account for time averaging effects on dispersion (Sykes and Gabruk, 1997). First, a velocity scale is defined as follows:

$$V = \sqrt{\bar{u}^2 + \bar{v}^2 + \langle u'u' \rangle + \langle v'v' \rangle + \langle w'w' \rangle}$$

An averaging length scale is then calculated from the velocity scale:

$$L_{avg} = 0.03\,V\,T_{avg}$$

where T_{avg} is the time average in seconds (either 5-minutes or 30-minutes for our simulations), and the 0.03 factor was determined empirically by Sykes and Gabruk (1997) using time-averaged dispersion observations.

A buoyancy-driven length scale is defined as a fraction of the mixed layer depth:

$$L_B = 0.3 z_i$$

when the heat flux is greater than or equal to zero, otherwise it represents horizontal meander under stable conditions:

$$L_B = 1000\,\text{m}$$

where z_i is the mixing depth (PBL height). At heights greater than z_i, L_B is assumed to be 1000 meters.

If the average length scale is less than the buoyancy-driven length scale ($L_{avg} < L_B$), then the buoyancy-driven velocity fluctuations were adjusted as follows:

$$VV = VV \left(\frac{L_{avg}}{L_B} \right)^{2/3}$$

A shear-driven length scale inside the boundary layer is defined as:

$$L_S = \frac{1}{\sqrt{\left(\dfrac{1}{0.3 z_i}\right)^2 + \left(\dfrac{1}{0.65 z}\right)^2}}$$

At heights greater than z_i, L_S is assumed to be 10 meters. If the average length scale is less than the shear-driven length scale ($L_{avg} < L_S$), then the shear-driven velocity fluctuations were adjusted as follows:

$$UU = UU \left(\frac{L_{avg}}{L_S} \right)^{2/3}$$

u_* is not output directly by HPAC. Therefore, u_* was calculated as follows:

$$u_* = \left(-\frac{\kappa g H_0 L}{\rho c_p T} \right)^{1/3}$$

where,

    L is the Monin-Obukhov Length
    κ is von Karman's constant
    g is the acceleration due to gravity

HPAC "sampler" locations were the same sites used for the MM5 runs, as listed in Table 1. For the profiles, the average MM5 height at all 12 locations was used, in addition to a 1 meter and a 10 meter height. The heights used in the profile samplers are shown in Table B-2. The heights used in the time series sampler file are shown in Table B-3. Note that there was no time series observed data for the following locations: B1, B4, B5, and B6 (sites 2, 3, 4, and 5 in Table 1). The only variables that were plotted for two different heights at the ISFF sites were wind speed and wind direction.

Table B-2. Heights in HPAC Profile Sampler File

No.	Height (m)	No.	Height (m)	No.	Height (m)	No.	Height (m)
1	1	32	752.04	63	1518.64	94	2967.39
2	10	33	776.76	64	1543.37	95	3092.66
3	29.68	34	801.47	65	1568.07	96	3217.94
4	59.36	35	826.23	66	1592.77	97	3363.59
5	84.09	36	850.99	67	1617.51	98	3509.24
6	108.82	37	875.69	68	1642.25	99	3677.1
7	133.6	38	900.38	69	1666.96	100	3844.96
8	158.37	39	925.12	70	1691.68	101	4037.33
9	183.1	40	949.86	71	1716.43	102	4229.7
10	207.82	41	974.59	72	1741.17	103	4468.8
11	232.56	42	999.31	73	1765.90	104	4707.91
12	257.29	43	1024.08	74	1790.63	105	5000.95
13	282.05	44	1048.84	75	1815.34	106	5294
14	306.82	45	1073.55	76	1840.05	107	5643.82
15	331.54	46	1098.25	77	1864.78	108	5993.64
16	356.27	47	1122.99	78	1889.52	109	6404.92
17	380.99	48	1147.74	79	1914.23	110	6816.21
18	405.71	49	1172.46	80	1938.95	111	7296.18
19	430.47	50	1197.19	81	1973.77	112	7776.15
20	455.23	51	1221.91	82	2008.59	113	8315.16
21	479.94	52	1246.63	83	2053.64	114	8854.17
22	504.65	53	1271.37	84	2098.68	115	9471.04
23	529.4	54	1296.12	85	2155.57	116	10087.9
24	554.15	55	1320.86	86	2212.46	117	10784.55
25	578.89	56	1345.59	87	2286.67	118	11481.21
26	603.64	57	1370.31	88	2360.87	119	12265.57
27	628.38	58	1395.03	89	2453.69	120	13049.94
28	653.12	59	1419.74	90	2546.51	121	13994.73
29	677.85	60	1444.45	91	2647.96	122	14939.51
30	702.58	61	1469.18	92	2749.42	123	16043.84
31	727.31	62	1493.92	93	2858.40	124	17148.17
						125	18420.47

Table B-3. Heights in HPAC Time Series Sampler File

Location	Height (m)
Central Facility	4
Central Facility	60
Smileyberg, KS	2.1
Smileyberg, KS	10
Brainard, KS	2.1
Brainard, KS	10
ISFF1	2.5
ISFF1	10
ISFF2	3.43
ISFF2	10

ISFF3	2.7
ISFF3	10
ISFF4	2.6
ISFF4	10
ISFF5	5
ISFF5	10
ISFF6	4.9
ISFF6	10
ISFF7	2.7
ISFF7	10
ISFF8	4.6
ISFF8	10
ISFF9	4.7
ISFF9	10

HPAC simulations were run for 24 hours for each of the three IHOP days (May 29, June 6 and June 7). To compare to the observed profile data, the 5-minute average MM5 MEDOC file was used with the profile sampler files. To compare to the time series data for the Central Facility, Smileyberg and Brainard, the 30-minute average MM5 MEDOC file was used with the time series sampler file. An additional set of runs using the 5-minute time average data was simulated in order to compare to the time series data at the 9 ISFF sites, since the observed data is every 5 minutes.

The domain was the same as the MM5 simulation. Default settings were used in HPAC as shown in Table B-4.

Table B-4. Default Settings Used in HPAC Simulations

Variable	Value	Units
Calm Turbulence	0.25	m^2/s^2
Calm Length Scale	1000	m
Stable Turbulence	0.01	m^2/s^2
Stable Length Scale	10	m
Stable Dissipation Rate	4.E-4	m^2/s^3
Boundary Layer Points	11	---
Conditional Averaging	Default	---
Max Time Step	900	Seconds

Reference:

Sykes, R. I. and R. S. Gabruk 1997: A second-order closure model for the effect of averaging time on turbulent plume dispersion. *J. Appl. Met.,* 36, 165-184.